hep-lat/0007014
UTHEP-428
UTCCP-P-90

Chiral properties of domain-wall quarks in quenched QCD

CP-PACS Collaboration : A. Ali Khan[1], S. Aoki[2], Y. Aoki[1,2], R. Burkhalter[1,2], S. Ejiri[1], M. Fukugita[3], S. Hashimoto[4], N. Ishizuka[1,2], Y. Iwasaki[1,2], T. Izubuchi[5], K. Kanaya[1,2], T. Kaneko[4], Y. Kuramashi[6], T. Manke[1], K. I. Nagai[1], J. Noaki[1], M. Okawa[4], H.P. Shanahan[1], Y. Taniguchi[2], A. Ukawa[1,2] and T. Yoshié[1,2]

[1]*Center for Computational Physics, University of Tsukuba, Tsukuba, Ibaraki 305-8577, Japan*
[2]*Institute of Physics, University of Tsukuba, Tsukuba, Ibaraki 305-8571, Japan*
[3]*Institute for Cosmic Ray Research, University of Tokyo, Tanashi, Tokyo 188-8502, Japan*
[4]*High Energy Accelerator Research Organization (KEK), Tsukuba, Ibaraki 305-0801, Japan*
[5]*Department of Physics, Kanazawa University, Kanazawa, Ishikawa 920-1192, Japan*
[6]*Department of Physics, Washington University, St. Louis, Missouri 63130*

(March 16, 2006)

Abstract

We investigate the chiral properties of quenched domain-wall QCD (DWQCD) at the lattice spacings $a^{-1} \simeq 1$ and 2 GeV for both plaquette and renormalization-group (RG) improved gauge actions. In the case of the plaquette action we find that the quark mass defined through the axial Ward-Takahashi identity remains non-vanishing in the DWQCD chiral limit that the bare quark mass $m_f \to 0$ and the length of the fifth dimension $N_s \to \infty$, indicating that chiral symmetry is not realized with quenched DWQCD up to $a^{-1} \simeq 2$ GeV. The behavior is much improved for the RG-improved gauge action: while a non-vanishing quark mass remains in the chiral limit at $a^{-1} \simeq 1$ GeV, the result at $a^{-1} \simeq 2$ GeV is consistent with an exponentially vanishing quark mass in the DWQCD chiral limit, indicating the realization of exact chiral symmetry. An interpretation and implications are briefly discussed.

I. INTRODUCTION

A recent exciting development in lattice field theory is the realization of exact chiral-like symmetry at finite lattice spacing without fermion doubling. It started with the domain-wall [1,2] and the overlap [3] formalisms, which were originally proposed to formulate chiral gauge theories. They were soon applied to vector gauge theories such as QCD [4–7], and progress culminated in the recent discovery [8] that the essential feature of these formalisms is the existence of chiral-like symmetry which follows from the Ginsparg-Wilson relation [9]. An explicit form of the fermion action satisfying this relation is already known [6]. These developments lead us to expect that QCD with exact chiral symmetry can be numerically simulated on a lattice.

The domain-wall fermion formalism is a five dimensional extension of the Wilson fermion action with a negative mass $-M$. The theoretical basis is that the effective four-dimensional theory obtained by integrating out the heavy unphysical modes satisfies the Ginsparg-Wilson relation [10,11]. On the practical side, the knowledge accumulated on the Wilson fermion action over the past twenty years enables an efficient implementation of this system on computers.

There are, however, two subtleties that need to be clarified for numerical applications of the domain wall formalism to QCD (DWQCD). First, the length of the fifth dimension, N_s, cannot be set to infinity: one has to study the finite N_s effect. Second, one has to tune the domain-wall height (i.e., fifth dimensional mass) M to an appropriate value in order to keep the massless mode.

In the free theory one massless mode exists in the range $0 < M < 2$ [4]. The two chiral modes, with opposite chiralities, are exponentially bound to the opposite boundaries in the fifth dimension. The situation remains unchanged in perturbation theory. An explicit calculation at one-loop order shows [12,13] the existence of the massless mode guaranteed for the range $0 < M' < 2$ where M' receives a shift by the one-loop quantum correction. It is also easy to demonstrate that finite N_s effects are suppressed exponentially in N_s.

Numerical tests of chiral properties and physical applications of (quenched) DWQCD were first discussed in Ref. [14]. Through measurements of pion mass and the K^0–$\overline{K}^0$ mixing matrix element at the gauge coupling $\beta = 6/g^2 \sim 6.0$ ($a^{-1} \approx 2$GeV), these quantities were shown to vanish in the chiral limit, as required by chiral symmetry, for a rather small fifth dimensional length of $N_s \sim 10$. Good chiral behavior has also been observed for $N_s \sim 10$ for a gauge field background with non-trivial topology [15]. Even the Atiyah-Singer index theorem has been shown to be approximately satisfied on a lattice for a non-zero quark mass [15,16].

These successful results have promoted further applications. The calculations include the strange quark mass using nonperturbative renormalization factors [17–19], the pion decay constant [20], the hadron mass spectrum [21,22] and QCD thermodynamics with dynamical quarks [23–25].

Earlier studies with DWQCD were limited to lattice spacings of around $a^{-1} \approx 2$ GeV. It is obviously necessary to investigate the scaling behavior and carry out the continuum extrapolation. Reducing the lattice spacing from $a^{-1} \simeq 2$ GeV, however, is computationally difficult, since the formalism requires N_s times more CPU time than usual simulations. Simulations at coarser lattices are easier, but we must clarify how large one can increase the

lattice spacing while keeping the massless mode.

The chiral properties of quenched DWQCD have been examined in a number of recent reports [22,26–28] employing large fifth dimensional lengths up to $N_s \sim 50$. The authors of Refs. [22,26], who made a study with the plaquette gauge action at $\beta = 5.7$ and 5.85 ($a^{-1} \approx 1 - 1.5$ GeV), claim that pion mass at such strong couplings does not vanish in the chiral limit after the $N_s \to \infty$ extrapolation, indicating that exact chiral symmetry is not realized. Our own study at $\beta = 5.65$ [28] yields the same conclusion. We also find that a renormalization-group (RG) improved gluon action [29] does not improve the situation at $a^{-1} \sim 1$ GeV [28].

In this paper we present a more systematic study of the chiral property of DWQCD covering both strong and 'weak' coupling regions, corresponding to lattice spacings $a^{-1} \simeq 1$ and 2 GeV with both plaquette and RG improved actions. We emphasize that the chiral properties are best studied with the quark mass extracted by the Ward-Takahashi (WT) identity for the axial vector current. The difference of this mass and the bare quark mass defines what we call 'anomalous quark mass'. We discuss that this quantity suffers from much less systematic uncertainties than the pion mass from both theoretical and numerical points of view. We study the behaviors of the anomalous quark mass as a function of N_s and examine whether it vanishes exponentially in the $N_s \to \infty$ limit for various coupling regimes, as required by the self-consistency of the proper chiral theory. This study is also made with varying M and a four dimensional spatial extent at some fixed coupling. We carry out this study with a parallel set of simulations employing both plaquette and RG-improved gauge actions to see the effect of improvement of the gauge field dynamics on the chiral property. In connection to our work we refer to Ref. [27], which attempts to extract the WT identity quark mass from the pseudoscalar susceptibility.

This paper is organized as follows. In section II we define the action and the anomalous quark mass. Numerical simulations and run parameters are described in section III. In section IV we investigate the chiral property for the plaquette action, and in section V for the RG-improved gauge action. Our provisional interpretation is given in section VI for the results we found from the simulation. We close the paper with a brief summary and comments on the application of DWQCD (section VII). Appendix A presents an analysis with pion mass, and discuss whether they support the conclusions based on the anomalous quark mass. Numerical data for the anomalous quark mass and pion mass are collected in Appendix B.

II. ACTION AND AXIAL WARD-TAKAHASHI IDENTITY

We adopt Shamir's domain-wall fermion action [4,5], except that the Wilson term and the domain wall height M have minus signs:

$$S_f = -\sum_{x,s,y,s'} \overline{\psi}(x,s) D_{dwf}(x,s;y,s') \psi(y,s') + \sum_x m_f \overline{q}(x) q(x) \ , \tag{II.1}$$

$$D_{dwf}(x,s;y,s') = D^4(x,y)\delta_{s,s'} + D^5(s,s')\delta_{x,y} + (M-5)\delta_{x,y}\delta_{s,s'} \ , \tag{II.2}$$

$$D^4(x,y) = \sum_\mu \frac{1}{2}\left[(1-\gamma_\mu) U_{x,\mu}\delta_{x+\hat{\mu},y} + (1+\gamma_\mu) U^\dagger_{y,\mu}\delta_{x-\hat{\mu},y}\right] , \tag{II.3}$$

$$D^5(s,s') = \begin{cases} P_L\delta_{2,s'} & (s=1) \\ P_L\delta_{s+1,s'} + P_R\delta_{s-1,s'} & (1<s<N_s) \\ P_R\delta_{N_s-1,s'} & (s=N_s) \end{cases}, \tag{II.4}$$

where x, y are four-dimensional space-time coordinates, and s, s' are fifth-dimensional or "flavor" index, bounded as $1 \le s, s' \le N_s$ with the free boundary condition at both ends (we assume N_s to be even); $P_{R/L}$ is the projection matrix $P_{R/L} = (1 \pm \gamma_5)/2$, and m_f is physical quark mass.

In DWQCD the zero mode of a domain-wall fermion is extracted by the "physical" quark field defined on the edges of the fifth dimensional space,

$$\begin{aligned} q(x) &= P_L\psi(x,1) + P_R\psi(x,N_s), \\ \overline{q}(x) &= \overline{\psi}(x,N_s)P_L + \overline{\psi}(x,1)P_R. \end{aligned} \tag{II.5}$$

The QCD operators are constructed from these quark fields.

For the gauge part of the action we employ the following form in 4 dimensions:

$$S_{\rm gluon} = \frac{1}{g^2}\left\{ c_0 \sum_{plaquette} {\rm Tr}U_{pl} + c_1 \sum_{rectangle} {\rm Tr}U_{rtg} + c_2 \sum_{chair} {\rm Tr}U_{chr} + c_3 \sum_{parallelogram} {\rm Tr}U_{plg} \right\}, \tag{II.6}$$

where the first term represents the standard plaquette action, and the remaining terms are six-link loops formed by a 1×2 rectangle, a bent 1×2 rectangle (chair) and a 3-dimensional parallelogram. The coefficients $c_0, \cdots, c_3$ satisfy the normalization condition

$$c_0 + 8c_1 + 16c_2 + 8c_3 = 1. \tag{II.7}$$

The standard Wilson plaquette action is given by $c_0 = 1, c_1 = c_2 = c_3 = 0$. The RG-improved action of Iwasaki [29] is defined by setting the parameters to $c_0 = 3.648, c_1 = -0.331, c_2 = c_3 = 0$: with this choice of parameters the action is expected to realize smooth gauge field fluctuations approximating those in the continuum limit better than with the unimproved plaquette action.

The chiral transformation of domain wall fermion is defined as [5],

$$\delta\psi(x,s) = iQ(s)\epsilon^a T^a \psi(x,s), \tag{II.8}$$

$$\delta\overline{\psi}(x,s) = -i\overline{\psi}(x,s)Q(s)\epsilon^a T^a, \tag{II.9}$$

where $Q(s) = {\rm sign}(N_s - 2s + 1)$, T^a is a generator of flavor symmetry group ${\rm SU}(N_f)$ with ϵ^a a transformation parameter. The corresponding WT identity becomes

$$\sum_\mu \left\langle \nabla_\mu A^a_\mu(x)\mathcal{O} \right\rangle = 2m_f \left\langle P^a(x)\mathcal{O}\right\rangle + 2\left\langle J^a_{5q}(x)\mathcal{O}\right\rangle + i\left\langle \delta^a_x\mathcal{O}\right\rangle, \tag{II.10}$$

where the axial-vector current $A^a_\mu(x)$ and the pseudoscalar density $P^a(x)$ are defined by

$$\begin{aligned} A^a_\mu(x) = \sum_s Q(s)\frac{1}{2}\Big(&\overline{\psi}(x,s)T^a(1-\gamma_\mu)U_\mu(x)\psi(x+\mu,s) \\ &-\overline{\psi}(x+\mu,s)(1+\gamma_\mu)U^\dagger_\mu(x)T^a\psi(x,s)\Big), \end{aligned} \tag{II.11}$$

$$P^a(x) = \overline{q}(x)T^a\gamma_5 q(x), \tag{II.12}$$

and $J^a_{5q}(x)$ representing explicit breaking of chiral symmetry takes the form,

$$J^a_{5q}(x) = -\overline{\psi}(x, \frac{N}{2})T^a P_L \psi(x, \frac{N}{2}+1) + \overline{\psi}(x, \frac{N}{2}+1)T^a P_R \psi(x, \frac{N}{2}). \tag{II.13}$$

For a smooth gauge field background the anomalous contribution $\left\langle J^a_{5q}(x)\mathcal{O}^b(y)\right\rangle$ is bounded by an exponentially small value with the argument $-N_s$ and vanishes in the limit $N_s \to \infty$ [5]. In this paper we adopt the operator $\mathcal{O} = P^b(0,\mathbf{0})$, and measure the chiral symmetry breaking effect by

$$m_{5q} = \lim_{t\to\infty} \frac{\sum_{\mathbf{x}} \left\langle J^a_{5q}(t,\mathbf{x})P^b(0,\mathbf{0})\right\rangle}{\sum_{\mathbf{x}} \left\langle P^a(t,\mathbf{x})P^b(0,\mathbf{0})\right\rangle}, \tag{II.14}$$

which we call 'anomalous quark mass'. We expect this quantity to be dominated by short-range fluctuations since it is determined by the coupling strength of pion to the operators J^a_{5q} and P^b. Therefore, finite-size effects are likely to be small. For the same reason, there should be no quenched chiral singularities in the relation between m_{5q} and the bare quark mass m_f.

The axial WT identity is written in terms of the anomalous quark mass as,

$$\frac{\sum_{\mathbf{x}} \nabla_\mu \left\langle A^a_\mu(t,\mathbf{x})P^b(y)\right\rangle}{2\sum_{\mathbf{x}} \left\langle P^a(t,\mathbf{x})P^b(y)\right\rangle} = m_f + m_{5q}. \tag{II.15}$$

The left-hand side of this equation, proportional to the pion mass squared, vanishes at $m_f + m_{5q} = 0$.

III. RUN PARAMETERS AND MEASUREMENTS

We explore the chiral properties of DWQCD at both $a^{-1} \simeq 1$ and 2 GeV using the plaquette and the RG-improved actions. For the plaquette action, we choose the couplings $\beta = 5.65$ and 6.0, which correspond to $a^{-1} = 1.00$ and 2.00 GeV, respectively, if one determines the scale from the string tension σ [30] assuming $\sigma = (440\ \mathrm{MeV})^2$. For the RG-improved action, we take $\beta = 2.2$ and 2.6 for which $a^{-1} = 0.97$ and 1.94 GeV also from the string tension reported in Refs. [31–33].

We generate quenched gauge configurations on four-dimensional $N_\sigma^3 \times N_\tau$ lattices. One sweep of the gauge update contains one pseudo-heatbath and four overrelaxation steps. For runs at $a^{-1} \simeq 1$ GeV we adopt the lattice size of $12^3 \times 24$ and $16^3 \times 24$ to study finite-size effects. At $a^{-1} \simeq 2$ GeV only a $16^3 \times 32$ lattice is employed. After a thermalization of 500 (2000) sweeps hadron propagators are calculated at every 100th (200th) sweeps for $a^{-1} \simeq 1$ GeV (2 GeV).

The domain-wall quark propagator is calculated on $N_\sigma^3 \times N_\tau \times N_s$ lattices, where the gauge configuration on each fifth dimensional coordinate s is identical and is fixed to the Coulomb gauge. The size of the fifth dimension is varied from $N_s = 10$ to 50 at $a^{-1} \simeq 1$ GeV, and from $N_s = 4$ to $24 - 30$ at $a^{-1} \simeq 2$ GeV, depending on the gauge action.

To allow a chiral extrapolation, we employ fermion masses of $m_f = 0.03, 0.05, 0.1$ (at $a^{-1} \simeq 1$ GeV) and $m_f = 0.02, 0.04, 0.06$ (at $a^{-1} \simeq 2$ GeV). The domain-wall height dependence is examined at $a^{-1} \simeq 1$ GeV with the choice of $M = 1.3, 1.7, 2.1$, and 2.5. At $a^{-1} \simeq 2$ GeV we choose $M = 1.8$.

The propagators are calculated with the conjugate gradient algorithm with an even-odd pre-conditioning. We place the source at $s = 1$ and N_s in the fifth coordinate, so that the propagator from the physical field $\overline{q}$ to the domain-wall field $\psi_{x,s}$ for arbitrary (x, s) is obtained. Both local and exponentially smeared sources are employed in the spatial directions, and meson masses are measured for all possible combinations of quark masses while only degenerate combinations are evaluated for anomalous quark masses.

Our simulation parameters and the number of configurations are given in Table I. We note that gauge configurations are generated independently for each choice of N_s and M, *i.e.,* there are no correlations between the data generated with a different domain-wall height and a fifth-dimensional size.

In Figs. 1 and 2 we show typical data for the ratio of two-point functions defined in (II.14) as a function of the temporal distance t. We obtain the anomalous quark mass m_{5q} at each m_f, M and N_s, by fitting the plateau with a constant, the fitting range being determined by the inspection of plots for the ratio and those for the effective pion mass. We choose $8 \leq t \leq 16$ as the fitting range for all simulations at $\beta = 5.65$ (plaquette) and $\beta = 2.2$ (RG). We use $10 \leq t \leq 22$ at $\beta = 6.0$ for the plaquette action and $\beta = 2.6$ for the RG action. The numerical values for m_{5q} and pion mass are given in Appendix B.

IV. PLAQUETTE GAUGE ACTION

We discuss the anomalous quark mass for the plaquette gauge action. The bare quark mass (m_f) dependence of the anomalous quark mass m_{5q} is illustrated in Fig. 3 for $\beta = 5.65$ and 6.0. We observe only a mild dependence of m_{5q} on m_f. The anomalous quark mass in the nominal chiral limit $m_{5q}(m_f = 0, N_s, M)$ is obtained by a linear extrapolation in m_f. The extrapolated values are collected in Appendix B.

If chiral symmetry is realized in the $N_s \to \infty$ limit of the DWQCD system, $m_{5q}(m_f = 0, N_s, M)$ should vanish exponentially in N_s. We examine this point first at a strong coupling $\beta = 5.65$ corresponding to $a^{-1} \simeq 1$ GeV. The anomalous quark mass in the nominal chiral limit, $m_{5q}(m_f = 0, N_s, M)$, is plotted as a function of N_s in Fig. 4 for three values of M ($M = 1.3, 1.7, 2.1$). A comparison of the filled symbols taken on a $16^3 \times 24 \times N_s$ lattice with the open ones on a spatially smaller $12^3 \times 24 \times N_s$ lattice shows no significant finite-size effect between the two spatial sizes corresponding to $N_\sigma a \simeq 2$ and 3 fm.

The solid lines in Fig. 4 show the results of fitting data taken on a $16^3 \times 24 \times N_s$ lattice to an exponential with a constant, $c + \alpha e^{-\xi N_s}$. This fit reproduces all five data points with an acceptable χ^2/dof for both $M = 1.7$ (χ^2/dof = 1.1) and $M = 2.1$ (χ^2/dof = 2.2). In contrast an exponential fit without a constant, $\alpha e^{-\xi N_s}$, does not work, resulting in a large $\chi^2/\text{dof} > 30 - 60$ (dotted lines).

In order to examine the stability of the fit, we carry out fits to the four points excluding the data for the smallest fifth dimensional length $N_s = 10$. As seen in Table II, the data are again fitted well with an exponential plus a constant, but not without a constant. The constant c agrees between the five- and four-point fits within statistical errors.

Our data at $\beta = 6.0$ are shown in Fig. 5 where, for comparison, the result at $\beta = 5.65$ and $M = 1.7$ are recapitulated from Fig. 4. One generally expects that the domain-wall formulation works better at weaker couplings [5]. Indeed, the decrease of m_{5q} as a function of N_s is much more rapid at $\beta = 6.0$, giving m_{5q} an order of magnitude smaller at $\beta = 6.0$ than at $\beta = 5.65$:

$$m_{5q} = \begin{cases} 10.32(46)\ \text{MeV} & M = 1.7 \text{ at } \beta = 5.65 \\ 0.79(16)\ \text{MeV} & M = 1.8 \text{ at } \beta = 6.0. \end{cases} \tag{IV.1}$$

Nonetheless, we still observe a clear flattening of m_{5q} toward a large N_s. A plain exponential fit without a residual constant does not work. This is true even if we drop the $N_s = 4$ data. The fit including a constant is acceptable as shown by the solid lines in Fig. 5 (see Table II for details of χ^2 analyses).

As a further test for the presence of a non-zero constant, we extract the decay rate ξ in N_s not only at the chiral limit ($m_f = 0$) but also at a finite m_f. According to the transfer matrix description of DWQCD [5,10,11], the mass term, which appears only at the boundary in the fifth dimension, does not affect the large N_s dependence of m_{5q}; hence we expect that ξ does not depend on m_f. The decay rates ξ from a fit with an exponential and a constant are plotted in Fig. 6, which show that this expectation is well satisfied at a strong coupling, and within estimated errors also at a weaker coupling. The decay rate extrapolated to the chiral limit from finite m_f is consistent with the value directly extracted for $m_f = 0$, showing the consistency of the analysis.

We conclude that a residual constant remains in the anomalous quark mass in the $N_s \to \infty$ limit. The presence of a residual constant, even if it is small, means that quenched DWQCD does *not* realize the expected chiral symmetry for the plaquette action, at least, up to $a^{-1} \simeq 2$ GeV.

We remark that our conclusion differs from Ref. [20], which indicates that m_{5q} vanishes exponentially in N_s at $\beta = 6.0$ with the plaquette action. We find that the two data for m_{5q} are mutually consistent in the overlapping range of N_s (see Fig. 5, where open points are from Ref. [20] and the solid points denote our data). The choice of $N_s \leq 10$ in Ref. [20] was too small to observe the asymptotic flattening.

V. RENORMALIZATION GROUP IMPROVED ACTION

We may ascribe the failure in fulfilling chiral symmetry seen in the last section to the roughness of gauge configurations with the plaquette action at the lattice spacings we have studied. We suspect that the massless mode may exist on sufficiently smooth gauge configurations close to the continuum limit [34,35]. One way to realize smooth gauge configurations, yet keeping the lattice spacing coarse enough to make a computation feasible, is to employ improved gauge actions. So we discuss the case with the RG-improved gauge action [29] in this section.

The anomalous quark mass in the nominal chiral limit $m_{5q}(m_f = 0, N_s, M)$ is plotted as a function of N_s in Figs. 7 and 8. Fig. 7 compares a typical result at a strong coupling ($\beta = 2.2$) with that at a weaker coupling ($\beta = 2.6$). Fig. 8 displays the results at $\beta = 2.2$ for three different choices of M and for two different choices of the spatial lattice size N_σ. A comparison of solid points ($16^3 \times 24 \times N_s$ lattices) and open points ($12^3 \times 24 \times N_s$) verifies

the absence of a significant finite size effect at this β. In order to take the $N_s \to \infty$ limit we carry out exponential fits, with or without a constant, as we did for the plaquette action. The fit parameters are summarized in Table III.

We first discuss the results in the weak coupling region displayed in Fig. 7. As one can see from large values of χ^2/dof in Table III, neither $c + \alpha e^{-\xi N_s}$ ($\chi^2/\mathrm{dof} = 12.8$) nor $\alpha e^{-\xi N_s}$ ($\chi^2/\mathrm{dof} = 16.9$) fits the data well in so far as the point at $N_s = 4$ is included. This means that the leading exponential term does not dominate the two point correlators owing to a non-trivial overlap of quark wave functions between the two domain walls for this small N_s.

If the data at $N_s = 4$ are excluded, however, the four points for $N_s \geq 10$ are fitted equally well with either $c + \alpha e^{-\xi N_s}$ (solid line) or $\alpha e^{-\xi N_s}$ (dotted line) as seen in the figure. In fact, the fit with a constant yields $c = -0.71(63) \times 10^{-5}$, consistent with zero at one standard deviation; the four data points fall on $\alpha e^{-\xi N_s}$, indicating the realization of chiral symmetry.

We obtain a different result for a strong coupling. Solid lines in Fig. 8 show fits to all five data points with an exponential plus a constant. They provide reasonable fits to all data. On the other hand, a plain exponential does not fit the data.

Repeating the analysis for the four data points excluding $N_s = 10$, we still find the fit with a non-zero constant ($\chi^2/\mathrm{dof} = 0.1$) being much better than a plain exponential ($\chi^2/\mathrm{dof} = 4.0$) at $M = 2.1$. The constant c is consistent between the four- and five-point fits. This analyses supports the conclusion that chiral symmetry is not realized at $M = 2.1$. The four data points at $M = 1.7$, on the other hand, are fitted well with either of the two forms with $\chi^2/\mathrm{dof} < 1$. The constant c for the four-point fit is consistent with zero within two standard deviations. Thus the possibility that m_{5q} vanishes exponentially in N_s at $M = 1.7$ cannot be excluded from this analysis at $m_f = 0$ alone.

To further explore this issue, we attempt to fit the data for $m_f \neq 0$. We find that the plain exponential does not fit the data at non-zero m_f, leading to a large χ^2/dof as shown in Fig. 9. Since we expect the anomalous quark mass to depend little on m_f from the transfer matrix formalism of DWQCD, this suggests that the good fit we obtained without a constant at $m_f = 0$ is perhaps accidental. While further data are needed for a definitive conclusion, we think it likely that a non-zero anomalous quark mass also remains in the $N_s \to \infty$ limit at $M = 1.7$.

The value of the residual quark mass is small. From the five-point fit, we obtain

$$m_{5q} = 3.60(45)\ \mathrm{MeV} \quad \text{at } M = 1.7 \tag{V.1}$$

$$= 2.87(23)\ \mathrm{MeV} \quad \text{at } M = 2.1 \tag{V.2}$$

We finally show the decay rates ξ at finite m_f and $m_f = 0$ in Fig. 10. The decay rates at $\beta = 2.2$ are obtained by the five-point fit with a constant, while those at $\beta = 2.6$ employ plain exponential fits to the four data points. As expected, the decay rates depend little on m_f; their values at $m_f \neq 0$ are consistent with those at $m_f = 0$.

We conclude that the RG-improved action significantly improves the chiral behavior of DWQCD. While chiral symmetry is still not realized at $a^{-1} \simeq 1$ GeV, the residual anomalous quark mass is sizably reduced compared with that with the plaquette action. The results at a weaker coupling ($a^{-1} \simeq 2$ GeV) are consistent with the vanishing anomalous quark mass, supporting the realization of chiral symmetry with DWQCD.

VI. DISCUSSION

Let us now try to understand our findings. The anomalous quark mass m_{5q} vanishes exponentially in N_s if the eigenvalues of the transfer matrix in the fifth direction are strictly less than unity [5,10,34,35]. The occurrence of a unit eigenvalue, in turn, is in one-to-one correspondence with that of a zero eigenvalue of the four dimensional Hermitian Wilson-Dirac operator H_W [34,35] or more complicated one, $\hat{H}_W$, defined through the fifth dimensional transfer matrix $\hat{T}$ [5,10],

It has been argued that zero eigenvalues of H_W are related to the existence of the parity-flavor broken phases in ordinary lattice QCD with the Wilson quark action [36–40]. The connection follows from the identity for the parity-flavor order parameter $\langle \bar{q} i\gamma_5 \tau^3 q \rangle$ given by

$$\begin{aligned}
\lim_{H\to+0} \left\langle \bar{q} i\gamma_5 \tau^3 q \right\rangle &= -\lim_{H\to+0} \mathrm{Tr} \frac{i\gamma_5\tau^3}{D_W + i\gamma_5\tau^3 H} = -\lim_{H\to+0} \mathrm{tr} \left[\frac{i\gamma_5}{D_W + i\gamma_5 H} - \frac{i\gamma_5}{D_W - i\gamma_5 H} \right] \\
&= -i \lim_{H\to+0} \mathrm{tr} \left[\frac{1}{H_W + iH} - \frac{1}{H_W - iH} \right] \\
&= -i \lim_{H\to+0} \int d\,\lambda\, \rho_{H_W}(\lambda) \left\langle \lambda \left| \left(\frac{1}{\lambda + iH} - \frac{1}{\lambda - iH} \right) \right| \lambda \right\rangle \\
&= -i \int d\,\lambda\, \rho_{H_W}(\lambda)(-2\pi i)\delta(\lambda) = -2\pi\, \rho_{H_W}(0), \qquad \text{(VI.1)}
\end{aligned}$$

where H is an external field coupled to the order parameter, $H_W = \gamma_5 D_W$ with D_W the Wilson-Dirac operator, and $\rho_{H_W}(\lambda)$ is the density of the eigenvalues of H_W.

In Fig.11, the expected phase diagram is schematically drawn in the (β, M) plane, where $-M$ is the bare quark mass of the Wilson quark action. In the shaded regions the parity-flavor symmetry is broken spontaneously corresponding to a non-zero density of zero eigenvalues of H_W. At the critical lines that form the phase boundaries, the neutral pion mass vanishes. At a strong coupling ($\beta < \beta_c$) there are only two critical lines, while there exist ten of them at a weak coupling ($\beta > \beta_c$) and 5 points where two lines meet at $\beta = \infty$. Each point corresponds to one continuum limit, whose low energy spectra are composed of a part of sixteen fermion doublers.

For DWQCD to work we have to tune the domain-wall height M within the thick shaded region in Fig. 11 in order to avoid zero eigenvalues of H_W. In the weak coupling limit, this region is given by $0 < M < 2$. As the coupling increases, the range is shifted to a larger value of M and shrinks in width. Finally no massless fermion exists in the strong coupling region at $\beta < \beta_c$.

A naive interpretation of our results for DWQCD according to this picture would be that $\beta_c > 6.0$ for the plaquette action while $2.6 > \beta_c > 2.2$ for the RG-improved action, or in terms of the lattice spacing a_c^{-1} evaluated at $\beta = \beta_c$, $a_c^{-1} \gtrsim 2$ GeV for the former action and 2 GeV$\gtrsim a_c^{-1} \gtrsim$1 GeV for the latter.

This interpretation seems inconsistent with the quenched spectrum result for the plaquette action obtained in Ref. [39]; in this work, non-zero pion mass, signalling the parity conserving phase, was reported over the range $0.909(11) \le M \le 2.47(5)$ at $\beta = 6.0$, indicating $\beta_c < 6.0$. A possible explanation reconciling this apparent conflict is as follows. If the order parameter, eq. (VI.1), remains non-zero in the $H \to +0$ limit, the charged pions become massless Nambu-Goldstone modes associated with spontaneous parity-flavor

breaking in the infinite volume limit. The fact that m_{5q} in the proper chiral limit is tiny at $\beta = 6.0$ suggests that the magnitude of the order parameter is extremely small. Since the simulation in Ref. [39] is performed on a finite volume (16^3) without adding the external field H, it may be difficult to detect the existence of massless pions corresponding to such a small order parameter. The anomalous quark mass, m_{5q}, on the other hand, is very sensitive to the small eigenvalues of H_W, and hence to the non-zero order parameter. To clarify this issue, a more detailed study for the parity-flavor breaking phase of ordinary lattice QCD with the Wilson quark will be needed.

The actual dynamics inducing non-zero $\rho_{H_W}(0)$ may be complicated, possibly involving instantons. The relation between the spectral gap of the Hermitian Wilson-Dirac operator H_W and the instanton number has been extensively studied [41]. While a single instanton causes a zero eigenvalue of H_W only for a single value of M, an ensemble of instantons may lead to a non-zero density $\rho_{H_W}(0) \neq 0$. In particular unphysical short-distance topological dislocations, having an action less than that of physical instantons that are present for the plaquette action, may lead to such an effect [41]. They will lead to an anomalous quark mass even at $a^{-1} \simeq 2$ GeV as we have found in our simulations.

This mechanism may also explain the difference in the lattice spacing needed to realize chiral symmetry in DWQCD between the plaquette and RG-improved actions. The RG-improved gauge action suppresses unphysical dislocations by pushing the action above that of physical instantons [42]. Hence their influence on the density of zero-eigenvalues will be negligibly small compared to that for the plaquette action. Work exploring zero eigenvalues of the Wilson-Dirac operator for both gauge actions [43] should shed light on this interesting problem.

VII. CONCLUSIONS

We have investigated the chiral property of domain-wall QCD within the quenched approximation. We have defined the anomalous quark mass (axial WT identity quark mass) as an indicator for the realization of chiral symmetry. Our simulations have been made in both strong and weak coupling regions corresponding to $a^{-1} \simeq 1$ and 2 GeV, using the plaquette and RG-improved gauge actions. We have found that the anomalous quark mass remains non-zero in the DWQCD chiral limit, $m_f \to 0$ and $N_s \to \infty$ for the plaquette action for $a^{-1} \leq 2$ GeV. The magnitude of chiral symmetry breaking rapidly decreases with lattice spacing, but the exact chiral symmetry is not realized at least for this lattice spacing.

On the contrary, our analysis for the RG-improved action reveals a much improved chiral behavior. The anomalous quark mass vanishes exponentially with this action at $a^{-1} \simeq 2$ GeV, indicating that the exact chiral symmetry is realized. At $a^{-1} \simeq 1$ GeV the improvement of the chiral behavior is not sufficient to remove a non-zero anomalous quark mass.

Overall, quenched domain-wall QCD at $a^{-1} \simeq 1$ GeV appears no better than usual lattice QCD with the ordinary Wilson quark action. Since the effect of explicit chiral symmetry breaking is non-negligible, the operators relevant for the electroweak matrix elements mix nontrivially between different chiralities. There is no *a priori* reason to expect that these mixing coefficients are small.

The situation is better in the weak coupling region, e.g.,at $a^{-1} \simeq 2$ GeV. Even with the plaquette action, the chiral symmetry breaking effect is significantly smaller than the physical u, d quark masses, and hence may not seriously affect the chiral properties of weak matrix elements [19]. Moreover, the chiral property of DWQCD is distinctly improved with the RG action: not only the explicit breaking is shown to vanish exponentially in N_s, but also the size of the breaking effect at finite N_s is smaller. The improved gauge actions, such as the RG-improved one, should be a preferred choice for future numerical simulations for DWQCD.

ACKNOWLEDGMENTS

This work is supported in part by the Grants-in-Aid of Ministry of Education (Nos. 09304029, 10640246, 10640248, 11640250, 10740107, 11640250, 11640294, 11740162, 12640253, 12014202, 2373). AAK and TM are supported by the JSPS Research for the Future Program (No. JSPS-RFTF 97P01102). SE, KN and JN are JSPS Research Fellows.

REFERENCES

[1] D. Kaplan, Phys. Lett. **B288** (92) 342; Nucl. Phys. B (Proc. Suppl.) **30** (1993) 597.
[2] M. Golterman, K. Jansen and D. Kaplan, Phys. Lett. **B301** (93) 219.
[3] R. Narayanan and H. Neuberger, Nucl. Phys. **B443** (1995) 305.
[4] Y. Shamir, Nucl. Phys. **B406** (93) 90.
[5] V. Furman and Y. Shamir, Nucl. Phys. **B439** (95) 54.
[6] H. Neuberger, Phys. Lett. **B417** (1998) 141; Phys. Lett. **B427** (1998) 353.
[7] P. Hasenfratz, V. Laliena and F. Niedermayer, Phys. Lett. **B427** (1998) 125.
[8] M. Lüscher, Phys. Lett. **B428** (1998) 342.
[9] P. Ginsparg and K. Wilson, Phys. Rev. **D25** (1982) 2649.
[10] H. Neuberger, Phys. Rev. **D57** (1998) 5417.
[11] Y. Kikukawa and T. Noguchi, hep-lat/9902022.
[12] S. Aoki and Y. Taniguchi, Phys. Rev. **D59** (1999) 054510.
[13] S. Aoki, T. Izubuchi, Y. Kuramashi and Y. Taniguchi, Phys. Rev. **D59** (1999) 094505.
[14] T. Blum and A. Soni, Phys. Rev. **D56** (1997) 174; Phys. Rev. Lett. **79** (1997) 3595; hep-lat/9712004.
[15] For a review, see T. Blum, Nucl. Phys. B (Proc. Suppl.) **73** (1999) 167 and references there in.
[16] J. F. Lagae and D. K. Sinclair, Nucl. Phys. B (Proc. Suppl.) **83-84** (2000) 405.
[17] T. Blum, A. Soni and M. Wingate, Nucl. Phys. B (Proc. Suppl.) **73** (1999) 201; Phys. Rev. **D60** (1999) 114507
[18] M. Wingate *et al*, Nucl. Phys. B (Proc. Suppl.) **83-84** (2000) 221.
[19] C. Dawson *et al*, Nucl. Phys. B (Proc. Suppl.) **83-84** (2000) 854.
[20] S. Aoki, T. Izubuchi, Y. Kuramashi and Y. Taniguchi, Nucl. Phys. B (Proc. Suppl.) **83-84** (2000) 624; hep-lat/0004003.
[21] S. Sasaki *et al*, Nucl. Phys. B (Proc. Suppl.) **83-84** (2000) 206.
[22] L. Wu *et al*, Nucl. Phys. B (Proc. Suppl.) **83-84** (2000) 224.
[23] P. Chen, N. Christ, G. Fleming, A. Kaehler, C. Malureanu, R. Mawhinney, G. Siegert, C. Sui, P. Vranas and Y. Zhestkov, Nucl. Phys. B (Proc. Suppl.) **73** (1999) 456.
[24] P. Vranas *et al*, hep-lat/9903024.
[25] P. Vranas *et al*, Nucl. Phys. B (Proc. Suppl.) **83-84** (2000) 414.
[26] For a review, see P. Chen, N. Christ, G. Fleming, A. Kaehler, C. Malureanu, R. Mawhinney, G. Siegert, C. Sui, P. M. Vranas, Y. Zhestkov, hep-lat/9812011 and references there in.
[27] G. T. Fleming *et al*, Nucl. Phys. B (Proc. Suppl.) **83-84** (2000) 363.
[28] CP-PACS Collaboration: A. Ali Khan *et al*, Nucl. Phys. B (Proc. Suppl.) **83-84** (2000) 591.
[29] Y. Iwasaki, preprint, UTHEP-118 (Dec. 1983), unpublished.
[30] R. G. Edwards, U. M. Heller, and T. R. Klassen, Nucl. Phys. **B517** (1998) 377.
[31] Y. Iwasaki, K. Kanaya, T. Kaneko and T. Yoshie, Phys. Rev. **D56** (1997) 151.
[32] CP-PACS Collaboration: M. Okamoto *et al*, Phys. Rev. **D60** (1999) 094510.
[33] CP-PACS Collaboration: A. Ali Khan *et al*, Nucl. Phys. B (Proc. Suppl.) **83-84** (2000) 176.
[34] P. Hernandez, K. Jansen and M. Lüscher, Nucl. Phys. **B552** (1999) 363.
[35] Y. Kikukawa, hep-lat/9912056.

[36] S. Aoki, Phys. Rev. **D30** (1984) 2653; Phys. Rev. Lett. **57** (1986) 3136; Nucl. Phys. **B314** (1989) 79.
[37] R. Setoodeh, C. T. H. Davies and I. M. Barbour, Phys. Lett. **B213** (1988) 195.
[38] S. Aoki and A. Gocksch, Phys. Lett. **B231** (1989) 449.
[39] S. Aoki, T. Kaneda and A. Ukawa, Phys. Rev. **D56** (1997) 1808.
[40] S. Sharpe and R. L. Singleton, Jr, Phys. Rev. **D58** (1998) 074501.
[41] For a review, see R. G. Edwards, U. M. Heller, R. Narayanan, hep-lat/0001013 and references there in.
[42] Y. Iwasaki and T. Yoshie, Phys. Lett. **125B** (1983) 197;Phys. Lett. **131B** (1983) 159; S. Itoh, Y. Iwasaki and T. Yoshie, Phys. Lett. **147B** (1984) 141.
[43] CP-PACS Collaboration, in preparation.
[44] R. Gupta, G. Guralnik, G. W. Kilcup and S. R. Sharpe, Phys. Rev. **D43** (1991) 2003.
[45] S. Aoki, T. Umemura, M. Fukugita, N. Ishizuka, H. Mino, M. Okawa, and A. Ukawa, Phys. Rev. **D50** (1994) 486.

TABLES

	plaquette ($\beta = 5.65$)					RG ($\beta = 2.2$)				
N_s	10	20	30	40	50	10	20	30	40	50
M	$12^3 \times 24$									
1.3	20	20	20	**20**	**20**	20	20	20	**20**	**20**
1.7	30	20	20	**20**	**20**	30	30	20	**40**	**20**
2.1	30	30	30	**20**	**20**	30	30	20	**20**	**20**
2.5	30	20	20	-	10	30	30	20	-	-
M	$16^3 \times 32$									
1.3	**20**	**20**	-	-	**20**	**20**	-	**24**	-	**24**
1.7	**20**	**20**	**20**	**20**	**20**	**20**	**24**	**20**	**20**	**24**
2.1	**20**	**20**	**20**	**20**	**20**	**20**	**20**	**20**	**20**	**24**

	plaquette ($\beta = 6.00$)					RG ($\beta = 2.6$)				
N_s	4	10	16	20	30	4	10	16	20	24
M	$12^3 \times 24$									
1.8	**20**	**40**	**60**	**80**	**100**	**20**	**40**	**60**	**80**	**100**

TABLE I. Number of configurations for the plaquette action and the RG improved action(RG) for each N_s. The anomalous quark mass is measured only at the points where number of configurations is written in **boldface**.

β	M	fitting range	$c + \alpha e^{-\xi N_s}$				$\alpha e^{-\xi N_s}$		
		of N_s	c	α	ξ	χ^2/dof	α	ξ	χ^2/dof
5.65	1.7	10–50	0.01032(46)	0.115(5)	0.0947(44)	1.07	0.087(9)	0.0488(52)	59.1
		20–50	0.00918(107)	0.08(2)	0.077(12)	0.00193	0.051(7)	0.0337(41)	9.05
	2.1	10–50	0.00725 (63)	0.061(3)	0.0838(69)	2.23	0.050(4)	0.0438(46)	34.8
		20–50	0.00524 (149)	0.040(6)	0.056(13)	0.202	0.034(2)	0.0313(21)	2.27
6.0	1.8	4–30	0.000565 (147)	0.12 (1)	0.364 (22)	8.70	0.11 (2)	0.333 (38)	47.8
	1.8	10–30	0.000396 (79)	0.023 (6)	0.195 (25)	0.162	0.012 (3)	0.123 (19)	7.29

TABLE II. Exponential fit of the anomalous quark mass m_{5q} for the plaquette action. Strong coupling results at $\beta = 5.65$ are for the lattice size $16^3 \times 24$, and those at a weak coupling of $\beta = 6.0$ are for $16^3 \times 32$ lattice. Fits with all of the five date points are represented by the fitting range 10–50 and 4–30. Four-points fits without $N_s = 10$ data are represented by 20–50 and 10–30.

β	M	fitting range of N_s	$c+\alpha e^{-\xi N_s}$ c	α	ξ	χ^2/dof	$\alpha e^{-\xi N_s}$ α	ξ	χ^2/dof
2.2	1.7	10–50	0.00371(46)	0.071(9)	0.121(12)	3.03	0.045(9)	0.066(11)	35.7
		20–50	0.00230(107)	0.025(7)	0.0620(201)	0.00002	0.020(2)	0.0370(28)	0.936
	2.1	10–50	0.00296 (24)	0.036(3)	0.0979(74)	0.232	0.025(4)	0.0505(76)	21.0
		20–50	0.00278 (43)	0.03(1)	0.085(21)	0.113	0.014(2)	0.0328(51)	3.98
2.6	1.8	4–24	0.0000099 (71)	0.122(9)	0.501(15)	12.8	0.12(1)	0.498(17)	16.9
	1.8	10–24	−0.0000071(63)	0.014(3)	0.281(25)	0.00227	0.019(2)	0.312 (12)	0.799

TABLE III. Exponential fit of the anomalous quark mass m_{5q} for the RG-improved action. Strong coupling results at $\beta = 2.2$ are for the lattice size $16^3 \times 24$, and those at a weak coupling of $\beta = 2.6$ are for $16^3 \times 32$ lattice. Fits with all of the five date points are represented by the fitting range 10–50 and 4–30. Four-points fit without $N_s = 10$ data are represented by 20–50 and 10–24.

APPENDIX A: PION MASS

The pion mass is a standard quantity in examining the chiral property, and hence often studied in the context of DWQCD. Analyses of this observable, however, is not straightforward due to possible finite size effects, particularly for small pion masses, and difficulties associated with the chiral extrapolation because of chiral logarithms, which may be quite significant in quenched QCD. Numerically the pion mass has to be extracted from an exponential falloff of the pion propagator. Even though the pion propagator has the best statistical quality among hadron propagators, this procedure is more susceptible to statistical and systematic uncertainties than the determination of the anomalous quark mass which involves only a constant fit to a ratio of two kinds of propagators. For these reasons we have employed the anomalous quark mass in the main body of the present paper. In this appendix we present our results for the pion mass, and discuss to what extent they match with those obtained with the anomalous quark mass.

Typical results for pion mass squared $m_\pi^2(m_f, N_s, M)$ are plotted as a function of the averaged bare quark mass $m_f^{av} = (m_{f1} + m_{f2})/2$ for the plaquette action in Fig. 12. The result shows a good linear behavior in m_f^{av}. The pion mass in the chiral limit $m_f \to 0$ is therefore estimated by linearly extrapolating m_π^2 in m_f^{av}. The numerical values of the pion mass are collected in Appendix B.

Strong coupling region

We first discuss pion mass results at the strong coupling $a^{-1} \simeq 1$ GeV. In Fig. 13 we plot the pion mass squared m_π^2 in the chiral limit $m_f^{av} = 0$ as a function of N_s for the plaquette action at $\beta = 5.65$. Filled symbols are obtained on a lattice of spatial size $N_\sigma = 16$ and open ones with a spatial size of $N_\sigma = 12$. A similar figure for the RG-improved action is shown in Fig. 14.

Solid lines in these figures show results of fits by a form $c + \alpha e^{-\xi N_s}$ using all five points obtained on an $N_\sigma = 16$ lattice ($M = 1.7, 2.1$) or an $N_\sigma = 12$ lattice ($M = 1.3, 2.5$). They reproduce the data well for a non-zero c with an acceptable χ^2 as summarized in Tables IV and V. Therefore pion mass does not vanish in the chiral limit $m_f \to 0$ and $N_s \to \infty$ at $a^{-1} \simeq 1$ GeV for the plaquette and the RG-improved actions, which is consistent with the conclusions from the analysis of the anomalous quark mass.

In order to check our procedure of taking the chiral limit we interchange the order of the limits $m_f^{av} \to 0$ and $N_s \to \infty$. As shown by solid lines going through open circles in Fig. 15, we first make a fit of form $m_\pi^2(m_f^{av}, N_s) = c'(m_f^{av}) + \alpha e^{-\xi N_s}$ for each value of m_f^{av}. We note that the constant term has to be included in the fit of the pion mass at non-zero m_f. A linear chiral extrapolation $m_\pi^2(m_f^{av}, N_s = \infty) = c'(m_f^{av}) = d + \gamma m_f^{av}$ then yields $d = 0.0432(52)$, which agrees well with the value of $c = 0.0440(43)$ previously obtained. The commutativity of the two limits is summarized by two symbols "X" and "Y" in Fig. 15, where X represents $m_\pi^2(m_f^{av} = 0, N_s = \infty)$ given with $m_f \to 0$, then $N_s \to \infty$ and Y represents the pion mass with the limit $N_s \to \infty$, then $m_f \to 0$. These two values agree very well with each other. The same consistency check is also made for the RG-improved action.

The above analyses strongly support the conclusion that m_π does not vanish in the limit $m_f^{av} \to 0$ and $N_s \to \infty$. In order to examine finite spatial volume effects as a possible

origin of this non-zero mass, we compare the pion mass squared in the proper chiral limit $m_\pi^2(m_f^{av} \to 0, N_s \to \infty)$ for two kinds of lattice volumes $12^3 \times 24$ (open symbols) and $16^3 \times 24$ (filled symbols) in Fig. 16.

The circles and diamonds represent the results from the plaquette and the RG action, respectively. The horizontal triangles are results for the Nambu-Goldstone pion mass of the Kogut-Susskind quark action at $\beta = 5.7$ for a spatial lattice size of $N_\sigma = 12$ (open triangle) and $N_\sigma = 16$ (filled triangle) [44]. From comparison of these data points, we consider that there may be some finite size effects at $M = 1.7$, but that they are not large enough to explain non-zero values of pion mass for DWQCD at strong coupling.

Since there still remains a possibility that this non-zero mass is caused by the quenching effect, we adopt the WT identity mass as a better indicator to test the chiral property of DWQCD in the main body of this article.

Weak coupling region

Pion mass squared in the chiral limit $m_\pi^2(m_f = 0, N_s, M)$ is plotted in Fig. 17 for the plaquette action at $\beta = 6.0$ and in Fig. 18 for the RG-improved action at $\beta = 2.6$. The results have large errors, and do not show a clear trend as a function of N_s. However, the magnitude beyond $N_s = 10$ are comparable to the value obtained for the Nambu-Goldstone pion mass of the Kogut-Susskind fermion at $\beta = 6.0$ for the same spatial lattice size $16^3 \times 40$ (open circle) [44,45]. This indicates that these non-zero pion masses are mainly caused by finite spatial volume effects. Hence the chiral property of DWQCD cannot be studied by pion mass in the weak coupling region on this volume.

action	M	fitting range	$c + \alpha e^{-\xi N_s}$				$\alpha e^{-\xi N_s}$		
		of N_s	c	α	ξ	χ^2/dof	α	ξ	χ^2/dof
plaq.	1.7	10–50	0.04404(434)	0.51(3)	0.0836(62)	0.838	0.41(4)	0.0485(54)	16.1
		20–50	0.03946(829)	0.4(1)	0.071(16)	0.944	0.26(4)	0.0341(46)	3.63
	2.1	10–50	0.07796(464)	0.35(3)	0.0832(78)	0.761	0.29(3)	0.0293(54)	20.4
		20–50	0.0602(262)	0.21(5)	0.046(28)	0.00354	0.21(1)	0.0195(16)	0.523
RG	1.7	10–50	0.02549(321)	0.30(4)	0.109(14)	0.585	0.20(4)	0.0513(92)	8.65
		20–50	0.0191(105)	0.14(8)	0.063(38)	0.0661	0.10(1)	0.0300(46)	0.456
	2.1	10–50	0.04453(426)	0.20(4)	0.100(21)	0.553	0.14(2)	0.0285(66)	7.17
		20–50	0.04669(449)	0.5(1.1)	0.15(11)	0.677	0.10(2)	0.0167(59)	2.80

TABLE IV. Exponential fit of pion mass squared m_π^2 in strong coupling region at $M = 1.7$ and 2.1. The four-dimensional lattice size is $16^3 \times 24$. Fits with all of five data points are represented by the fitting range $10 - 50$ and four-points fits without $N_s = 10$ data are represented by $20 - 50$.

action	M	fitting range of N_s	$c+\alpha e^{-\xi N_s}$ c	α	ξ	χ^2/dof	$\alpha e^{-\xi N_s}$ α	ξ	χ^2/dof
plaq.	1.3	10–50	0.09328(709)	1.00(5)	0.0904(57)	0.702	0.8(1)	0.0500(64)	27.0
		20–50	0.0842(126)	0.7(2)	0.075(14)	0.147	0.45(7)	0.0320(50)	5.19
	1.7	10–50	0.0593(121)	0.6(1)	0.100(25)	5.27	0.40(6)	0.0454(74)	16.6
		20–50	−0.021(281)	0.2(2)	0.021(56)	4.90	0.22(3)	0.0267(49)	2.47
	2.1	10–50	0.08112(660)	0.43(6)	0.098(14)	0.226	0.31(4)	0.0332(65)	11.7
		20–50	0.0765(140)	0.3(2)	0.077(42)	0.192	0.20(2)	0.0189(35)	1.46
	2.5	10–50	0.14777(566)	0.6(2)	0.159(33)	0.617	0.29(6)	0.0205(86)	30.2
		20–50							
RG	1.3	10–50	0.03482(494)	0.83(7)	0.1125(84)	0.437	0.63(9)	0.0757(98)	11.4
		20–50	0.03175(973)	0.6(4)	0.098(34)	0.670	0.31(6)	0.0475(69)	2.23
	1.7	10–50	0.03681(390)	0.4(1)	0.150(31)	0.704	0.20(4)	0.048(11)	9.15
		20–50	0.0327(152)	0.1(2)	0.08(12)	1.30	0.08(2)	0.0189(60)	0.759
	2.1	10–50	0.0344(181)	0.13(2)	0.051(25)	0.281	0.15(1)	0.0262(35)	0.529
		20–50	−0.035(239)	0.2(2)	0.013(35)	0.1593	0.12(2)	0.0209(56)	0.0883

TABLE V. Exponential fit of the pion mass squared m_π^2 in strong coupling region at $M = 1.3, 1.7, 2.1, 2.5$. The four dimensional lattice size is $12^3 \times 24$. Fits with all of five data points are represented by the fitting range $10 - 50$ and four-points fit without $N_s = 10$ data are represented by $20 - 50$.

APPENDIX B

In this appendix we lists results for anomalous quark mass m_{5q} and pion mass squared m_π^2.

m_f	N_s				
	10	20	30	40	50
	$\beta = 5.65,\ M = 1.3$ on $12^3 \times 24$				
0.00	–	–	–	0.0605 (31)	0.0499 (20)
0.03	–	–	–	0.0622 (28)	0.0520 (19)
0.05	–	–	–	0.0629 (26)	0.0530 (19)
0.1	–	–	–	0.0658 (24)	0.0565 (21)
	$\beta = 5.65,\ M = 1.7$ on $12^3 \times 24$				
0.00	–	–	–	0.01303 (56)	0.01019 (47)
0.03	–	–	–	0.01304 (53)	0.01019 (42)
0.05	–	–	–	0.01302 (59)	0.01016 (42)
0.1	–	–	–	0.01302 (63)	0.01018 (44)
	$\beta = 5.65,\ M = 2.1$ on $12^3 \times 24$				
0.00	–	–	–	0.00934 (28)	0.00770 (42)
0.03	–	–	–	0.01031 (31)	0.00894 (29)
0.05	–	–	–	0.01051 (35)	0.00907 (33)
0.1	–	–	–	0.01230 (55)	0.01155 (64)

TABLE VI. Anomalous quark mass for the plaquette action in the strong coupling region at $\beta = 5.65,\ M = 1.3, 1.7, 2.1$ on $12^3 \times 24$ lattice.

m_f	N_s				
	10	20	30	40	50
	$\beta = 5.65$, $M = 1.3$ on $16^3 \times 24$				
0.00	0.1747 (16)	0.1129 (14)	–	–	0.04925 (98)
0.03	0.1723 (16)	0.1123 (16)	–	–	0.0513 (11)
0.05	0.1700 (17)	0.1111 (17)	–	–	0.0522 (11)
0.1	0.1660 (18)	0.1102 (20)	–	–	0.0557 (14)
	$\beta = 5.65$, $M = 1.7$ on $16^3 \times 24$				
0.00	0.05514 (49)	0.02717 (62)	0.01748 (55)	0.01303 (27)	0.01095 (47)
0.03	0.05373 (46)	0.02646 (58)	0.01721 (51)	0.01280 (29)	0.01092 (39)
0.05	0.05228 (49)	0.02561 (59)	0.01691 (51)	0.01252 (35)	0.01084 (43)
0.1	0.05002 (67)	0.02445 (60)	0.01645 (54)	0.01219 (52)	0.01080 (44)
	$\beta = 5.65$, $M = 2.1$ on $16^3 \times 24$				
0.00	0.03349 (31)	0.01820 (37)	0.01253 (39)	0.00954 (24)	0.00757 (43)
0.03	0.03338 (27)	0.01941 (35)	0.01358 (37)	0.01032 (22)	0.00880 (38)
0.05	0.03261 (28)	0.01947 (38)	0.01361 (37)	0.01032 (24)	0.00909 (46)
0.1	0.03254 (37)	0.02171 (56)	0.01542 (44)	0.01203 (56)	0.01124 (51)

TABLE VII. Anomalous quark mass for the plaquette action in the strong coupling region at $\beta = 5.65$, $M = 1.3, 1.7, 2.1$ on $16^3 \times 24$ lattice.

m_f	N_s				
	4	10	16	20	30
0.0	0.02955 (29)	0.00373 (13)	0.00148 (17)	0.00084 (11)	0.000467 (57)
0.02	0.02884 (25)	0.00360 (11)	0.00134 (14)	0.000750 (90)	0.000403 (49)
0.04	0.02804 (20)	0.003446 (78)	0.001128 (93)	0.000637 (73)	0.000317 (42)
0.06	0.02735 (18)	0.003316 (64)	0.000989 (66)	0.000548 (59)	0.000259 (38)

TABLE VIII. Anomalous quark mass for the plaquette action in the weak coupling region at $\beta = 6.0$, $M = 1.8$ on $16^3 \times 32$ lattice.

m_f	N_s				
	10	20	30	40	50
	$\beta = 2.2$, $M = 1.3$ on $12^3 \times 24$				
0.00	–	–	–	0.01565 (90)	0.01260 (81)
0.03	–	–	–	0.01605 (84)	0.01324 (78)
0.05	–	–	–	0.01657 (86)	0.01385 (80)
0.1	–	–	–	0.0172 (11)	0.01491 (84)
	$\beta = 2.2$, $M = 1.7$ on $12^3 \times 24$				
0.00	–	–	–	0.00413 (23)	0.00319 (26)
0.03	–	–	–	0.00399 (20)	0.00302 (24)
0.05	–	–	–	0.00403 (25)	0.00286 (25)
0.1	–	–	–	0.00377 (21)	0.00257 (26)
	$\beta = 2.2$, $M = 2.1$ on $12^3 \times 24$				
0.00	–	–	–	0.00378 (25)	0.00303 (24)
0.03	–	–	–	0.00386 (21)	0.00306 (19)
0.05	–	–	–	0.00373 (22)	0.00299 (17)
0.1	–	–	–	0.00388 (23)	0.00304 (24)

TABLE IX. Anomalous quark mass for the RG improved action in the strong coupling region at $\beta = 2.2$, $M = 1.3, 1.7, 2.1$ on $12^3 \times 24$ lattice.

m_f	N_s				
	10	20	30	40	50
	$\beta = 2.2$, $M = 1.3$ on $16^3 \times 24$				
0.00	0.09729 (99)	–	0.02340 (41)	–	0.01329 (48)
0.03	0.095 (1)	–	0.02345 (39)	–	0.01356 (49)
0.05	0.0928 (11)	–	0.02340 (41)	–	0.01378 (59)
0.1	0.0890 (11)	–	0.02350 (55)	–	0.01422 (75)
	$\beta = 2.2$, $M = 1.7$ on $16^3 \times 24$				
0.00	0.02486 (42)	0.00966 (35)	0.00626 (39)	0.00443 (28)	0.00344 (33)
0.03	0.02387 (38)	0.00920 (32)	0.00586 (35)	0.00412 (26)	0.00329 (28)
0.05	0.02281 (35)	0.00875 (33)	0.00549 (33)	0.00379 (23)	0.00321 (22)
0.1	0.02113 (35)	0.00800 (32)	0.00480 (33)	0.00326 (24)	0.00296 (20)
	$\beta = 2.2$, $M = 2.1$ on $16^3 \times 24$				
0.00	0.01633 (35)	0.00788 (30)	0.00490 (26)	0.00377 (25)	0.00314 (22)
0.03	0.01626 (29)	0.00804 (28)	0.00511 (21)	0.00381 (19)	0.00318 (18)
0.05	0.0158 (3)	0.00782 (29)	0.00501 (20)	0.00368 (18)	0.00312 (16)
0.1	0.01570 (28)	0.00811 (30)	0.00535 (21)	0.00374 (20)	0.00317 (19)

TABLE X. Anomalous quark mass for the RG improved action in the strong coupling region at $\beta = 2.2$, $M = 1.3, 1.7, 2.1$ on $16^3 \times 24$ lattice.

m_f	N_s				
	4	10	16	20	24
0.0	0.01649 (11)	0.000817 (20)	0.000146 (22)	0.000042 (11)	0.000009 (2)
0.02	0.016238 (99)	0.000812 (17)	0.000136 (17)	0.0000405 (87)	0.0000087 (15)
0.04	0.015920 (80)	0.000803 (16)	0.000116 (12)	0.0000397 (78)	0.0000090 (19)
0.06	0.015677 (70)	0.000801 (16)	0.0001060 (76)	0.0000387 (73)	0.0000089 (19)

TABLE XI. Anomalous quark mass for the RG improved action in the weak coupling region at $\beta = 2.6$, $M = 1.8$ on $16^3 \times 32$ lattice.

m_f	N_s				
	10	20	30	40	50
	$\beta = 5.65,\ M = 1.3$ on $12^3 \times 24$				
0.00	0.4982 (80)	0.2504 (83)	0.1618 (47)	0.1234 (71)	0.1007 (59)
0.03	0.5817 (81)	0.3197 (82)	0.2258 (45)	0.1845 (66)	0.1597 (61)
0.04	0.6078 (81)	0.3415 (82)	0.2462 (44)	0.2038 (63)	0.1787 (64)
0.05	0.6341 (82)	0.3635 (83)	0.2666 (43)	0.2233 (61)	0.1978 (66)
0.065	0.6760 (83)	0.3981 (84)	0.2987 (44)	0.2536 (61)	0.2272 (71)
0.075	0.7030 (83)	0.4206 (84)	0.3195 (43)	0.2736 (59)	0.2466 (72)
0.1	0.7733 (84)	0.4790 (85)	0.3733 (43)	0.3249 (59)	0.2964 (76)
	$\beta = 5.65,\ M = 1.7$ on $12^3 \times 24$				
0.00	0.2675 (55)	0.1292 (68)	0.0889 (61)	0.0833 (55)	0.0537 (50)
0.03	0.4190 (55)	0.2840 (61)	0.2440 (53)	0.2384 (54)	0.2114 (50)
0.04	0.4667 (57)	0.3329 (61)	0.2927 (53)	0.2882 (54)	0.2630 (54)
0.05	0.5148 (59)	0.3822 (61)	0.3416 (52)	0.3375 (52)	0.3147 (58)
0.065	0.5912 (62)	0.4589 (63)	0.4193 (55)	0.4171 (61)	0.3929 (64)
0.075	0.6401 (63)	0.5094 (62)	0.4692 (54)	0.4662 (59)	0.4453 (65)
0.1	0.7679 (65)	0.6401 (61)	0.6004 (56)	0.5966 (61)	0.5781 (69)
	$\beta = 5.65,\ M = 2.1$ on $12^3 \times 24$				
0.00	0.2418 (68)	0.1393 (61)	0.1067 (60)	0.0876 (68)	0.0839 (67)
0.03	0.4143 (70)	0.3206 (56)	0.2903 (55)	0.2719 (64)	0.2689 (64)
0.04	0.4722 (74)	0.3813 (57)	0.3521 (55)	0.3344 (65)	0.3327 (67)
0.05	0.5295 (77)	0.4416 (57)	0.4134 (55)	0.3962 (64)	0.3955 (69)
0.065	0.6175 (82)	0.5328 (62)	0.5056 (60)	0.4895 (69)	0.4888 (77)
0.075	0.6740 (83)	0.5929 (60)	0.5666 (58)	0.5505 (67)	0.5505 (76)
0.1	0.8172 (85)	0.7439 (58)	0.7195 (57)	0.7037 (68)	0.7037 (77)
	$\beta = 5.65,\ M = 2.5$ on $12^3 \times 24$				
0.00	0.2624 (63)	0.1701 (48)	0.1546 (43)	–	0.1430 (83)
0.03	0.4007 (59)	0.3049 (49)	0.2796 (43)	–	0.2439 (77)
0.04	0.4496 (59)	0.3535 (52)	0.3270 (46)	–	0.2894 (80)
0.05	0.4976 (59)	0.4012 (56)	0.3729 (49)	–	0.3320 (83)
0.065	0.5682 (61)	0.4698 (61)	0.4385 (54)	–	0.3880 (88)
0.075	0.6146 (60)	0.5153 (63)	0.4806 (56)	–	0.4236 (89)
0.1	0.7284 (60)	0.6239 (68)	0.5783 (60)	–	0.4984 (88)

TABLE XII. Pion mass squared for the plaquette action in the strong coupling region at $\beta = 5.65,\ M = 1.3, 1.7, 2.1, 2.5$ on $12^3 \times 24$ lattice.

m_f	N_s				
	10	20	30	40	50
	$\beta = 5.65,\ M = 1.3$ on $16^3 \times 24$				
0.00	0.499 (5)	0.2556 (40)	–	–	0.0957 (53)
0.03	0.5823 (52)	0.3257 (42)	–	–	0.1545 (50)
0.04	0.6084 (53)	0.3480 (43)	–	–	0.1734 (49)
0.05	0.6347 (54)	0.3704 (45)	–	–	0.1925 (48)
0.065	0.6766 (55)	0.4056 (47)	–	–	0.2215 (49)
0.075	0.7035 (56)	0.4284 (48)	–	–	0.2409 (48)
0.1	0.7737 (58)	0.4876 (50)	–	–	0.2905 (46)
	$\beta = 5.65,\ M = 1.7$ on $16^3 \times 24$				
0.00	0.2661 (49)	0.1358 (56)	0.0888 (36)	0.0599 (38)	0.0520 (31)
0.03	0.4179 (51)	0.2916 (55)	0.2434 (34)	0.2183 (32)	0.2086 (30)
0.04	0.4656 (53)	0.3411 (57)	0.2929 (37)	0.2693 (33)	0.2599 (35)
0.05	0.5137 (55)	0.3911 (59)	0.3426 (40)	0.3204 (33)	0.3113 (38)
0.065	0.5898 (58)	0.4687 (65)	0.4198 (46)	0.3992 (37)	0.3894 (47)
0.075	0.6392 (59)	0.5198 (64)	0.4707 (48)	0.4512 (36)	0.4414 (48)
0.1	0.7676 (61)	0.6513 (66)	0.6019 (53)	0.5849 (36)	0.5735 (54)
	$\beta = 5.65,\ M = 2.1$ on $16^3 \times 24$				
0.00	0.2317 (40)	0.1434 (33)	0.1132 (72)	0.0935 (50)	0.0815 (38)
0.03	0.4052 (46)	0.3247 (37)	0.2973 (62)	0.2792 (45)	0.2675 (43)
0.04	0.4629 (50)	0.3860 (42)	0.3604 (63)	0.3416 (49)	0.3317 (47)
0.05	0.5202 (55)	0.4464 (46)	0.4226 (62)	0.4034 (51)	0.3945 (51)
0.065	0.6085 (62)	0.5390 (52)	0.5166 (68)	0.4979 (58)	0.4902 (60)
0.075	0.6652 (65)	0.5982 (56)	0.5774 (63)	0.5589 (56)	0.5509 (61)
0.1	0.8095 (72)	0.7484 (60)	0.7299 (60)	0.7131 (54)	0.7036 (66)

TABLE XIII. Pion mass squared for the plaquette action in the strong coupling region at $\beta = 5.65,\ M = 1.3, 1.7, 2.1$ on $16^3 \times 24$ lattice.

m_f	N_s				
	10	20	30	40	50
	$\beta = 2.2,\ M = 1.3$ on $12^3 \times 24$				
0.00	0.3038 (55)	0.1208 (55)	0.0684 (71)	0.0415 (50)	0.0389 (60)
0.03	0.4002 (52)	0.2106 (52)	0.1579 (64)	0.1325 (47)	0.1253 (57)
0.04	0.4301 (52)	0.2388 (53)	0.1867 (63)	0.1619 (49)	0.1518 (59)
0.05	0.4604 (52)	0.2671 (54)	0.2154 (61)	0.1916 (49)	0.1786 (60)
0.065	0.5083 (52)	0.3120 (56)	0.2605 (64)	0.2363 (55)	0.2215 (64)
0.075	0.5395 (52)	0.3410 (56)	0.2894 (61)	0.2667 (53)	0.2494 (63)
0.1	0.6209 (51)	0.4169 (56)	0.3647 (58)	0.3433 (54)	0.3228 (60)
	$\beta = 2.2,\ M = 1.7$ on $12^3 \times 24$				
0.00	0.1304 (50)	0.0575 (50)	0.0405 (57)	0.0408 (42)	0.0302 (73)
0.03	0.2892 (51)	0.2186 (46)	0.2013 (54)	0.2049 (39)	0.1898 (57)
0.04	0.3394 (54)	0.2697 (48)	0.2529 (56)	0.2588 (40)	0.2410 (55)
0.05	0.3900 (57)	0.3210 (49)	0.3042 (58)	0.3119 (40)	0.2917 (51)
0.065	0.4695 (64)	0.4016 (55)	0.3850 (66)	0.3961 (48)	0.3724 (56)
0.075	0.5213 (64)	0.4540 (54)	0.4372 (68)	0.4486 (46)	0.4234 (53)
0.1	0.6559 (67)	0.5904 (56)	0.5737 (77)	0.5863 (47)	0.5582 (58)
	$\beta = 2.2,\ M = 2.1$ on $12^3 \times 24$				
0.00	0.1159 (64)	0.0810 (63)	0.0645 (68)	0.0556 (73)	0.0415 (82)
0.03	0.2879 (60)	0.2510 (55)	0.2303 (64)	0.2272 (71)	0.2131 (73)
0.04	0.3461 (63)	0.3083 (56)	0.2873 (66)	0.2848 (75)	0.2705 (74)
0.05	0.4038 (65)	0.3644 (58)	0.3429 (68)	0.3415 (78)	0.3274 (72)
0.065	0.4911 (72)	0.4519 (64)	0.4276 (76)	0.4292 (87)	0.4143 (81)
0.075	0.548 (7)	0.5068 (66)	0.4817 (73)	0.4851 (85)	0.4706 (76)
0.1	0.6906 (72)	0.6482 (71)	0.6198 (69)	0.6279 (84)	0.6136 (76)
	$\beta = 2.2,\ M = 2.5$ on $12^3 \times 24$				
0.00	0.1549 (48)	0.102 (6)	0.1127 (63)	–	–
0.03	0.2814 (47)	0.2208 (57)	0.2184 (53)	–	–
0.04	0.3256 (48)	0.2649 (57)	0.2611 (54)	–	–
0.05	0.3692 (51)	0.3076 (58)	0.3018 (53)	–	–
0.065	0.4329 (56)	0.3699 (59)	0.3607 (54)	–	–
0.075	0.4754 (59)	0.4099 (59)	0.3965 (52)	–	–
0.1	0.5793 (65)	0.5058 (58)	0.4797 (48)	–	–

TABLE XIV. Pion mass squared for the RG improved action in the strong coupling region at $\beta = 2.2,\ M = 1.3, 1.7, 2.1, 2.5$ on $12^3 \times 24$ lattice.

m_f	N_s				
	10	20	30	40	50
	$\beta = 2.2$, $M = 1.3$ on $16^3 \times 24$				
0.00	0.3126 (54)	–	0.0709 (19)	–	0.0464 (30)
0.03	0.4095 (56)	–	0.1609 (19)	–	0.1348 (28)
0.04	0.4400 (58)	–	0.1900 (19)	–	0.1634 (29)
0.05	0.4707 (59)	–	0.2190 (21)	–	0.1918 (30)
0.065	0.5194 (62)	–	0.2642 (25)	–	0.2368 (34)
0.075	0.5508 (63)	–	0.2938 (26)	–	0.2652 (34)
0.1	0.6326 (66)	–	0.3702 (33)	–	0.3395 (35)
	$\beta = 2.2$, $M = 1.7$ on $16^3 \times 24$				
0.00	0.1276 (49)	0.0579 (37)	0.0392 (36)	0.0308 (35)	0.0246 (35)
0.03	0.2882 (46)	0.2222 (34)	0.2012 (32)	0.1959 (33)	0.1908 (34)
0.04	0.3392 (45)	0.2763 (36)	0.2527 (35)	0.2498 (37)	0.2454 (36)
0.05	0.3905 (44)	0.3300 (38)	0.3042 (37)	0.3034 (40)	0.2995 (38)
0.065	0.4704 (46)	0.4131 (44)	0.3854 (42)	0.3874 (46)	0.3837 (44)
0.075	0.5228 (45)	0.4667 (45)	0.4381 (42)	0.4409 (48)	0.4378 (45)
0.1	0.6582 (45)	0.6046 (48)	0.5760 (47)	0.5798 (53)	0.5773 (47)
	$\beta = 2.2$, $M = 2.1$ on $16^3 \times 24$				
0.00	0.1194 (51)	0.0735 (40)	0.0539 (46)	0.0455 (41)	0.0492 (46)
0.03	0.2868 (42)	0.2442 (38)	0.2303 (45)	0.2177 (40)	0.2238 (44)
0.04	0.3425 (40)	0.302 (4)	0.2912 (49)	0.2754 (43)	0.2840 (48)
0.05	0.398 (4)	0.3590 (41)	0.3509 (51)	0.3324 (45)	0.3427 (49)
0.065	0.4826 (43)	0.4459 (47)	0.4413 (59)	0.4202 (53)	0.4336 (58)
0.075	0.5376 (43)	0.5019 (48)	0.4991 (58)	0.4763 (51)	0.4899 (56)
0.1	0.6770 (49)	0.6434 (54)	0.6445 (59)	0.6197 (51)	0.6336 (56)

TABLE XV. Pion mass squared for the RG improved action in the strong coupling region at $\beta = 2.2$, $M = 1.3, 1.7, 2.1$ on $16^3 \times 24$ lattice.

m_f	N_s				
	4	10	16	20	30
0.0	0.0891 (49)	0.0096 (36)	0.0025 (27)	0.0063 (21)	0.0019 (20)
0.02	0.1617 (43)	0.0795 (30)	0.0711 (24)	0.0736 (19)	0.0703 (17)
0.03	0.1959 (41)	0.1130 (34)	0.1032 (25)	0.1051 (20)	0.1029 (21)
0.04	0.2310 (39)	0.1471 (32)	0.1359 (24)	0.1371 (20)	0.1362 (20)
0.04	0.2311 (40)	0.1471 (36)	0.1362 (26)	0.1380 (21)	0.1366 (23)
0.05	0.2671 (38)	0.1823 (35)	0.1710 (27)	0.1714 (23)	0.1706 (20)
0.06	0.3041 (36)	0.2179 (34)	0.2059 (27)	0.2061 (23)	0.2059 (20)

TABLE XVI. Pion mass squared for the plaquette action in the weak coupling region at $\beta = 6.0$, $M = 1.8$ on $16^3 \times 32$ lattice.

m_f	N_s				
	4	10	16	20	24
0.0	0.0536 (26)	0.0044 (33)	0.0052 (23)	0.0023 (19)	0.0022 (16)
0.02	0.1188 (24)	0.0670 (30)	0.0671 (23)	0.0646 (15)	0.0652 (14)
0.03	0.1505 (26)	0.0967 (32)	0.0969 (26)	0.0942 (17)	0.0959 (15)
0.04	0.1826 (29)	0.1268 (30)	0.1270 (27)	0.1243 (17)	0.1268 (15)
0.04	0.1835 (29)	0.1274 (34)	0.1280 (29)	0.1246 (19)	0.1274 (16)
0.05	0.2150 (36)	0.1583 (31)	0.1582 (31)	0.1559 (18)	0.1580 (16)
0.06	0.2491 (39)	0.1907 (33)	0.1904 (31)	0.1877 (18)	0.1908 (16)

TABLE XVII. Pion mass squared for the RG improved action in the weak coupling region at $\beta = 2.6$, $M = 1.8$ on $16^3 \times 32$ lattice.

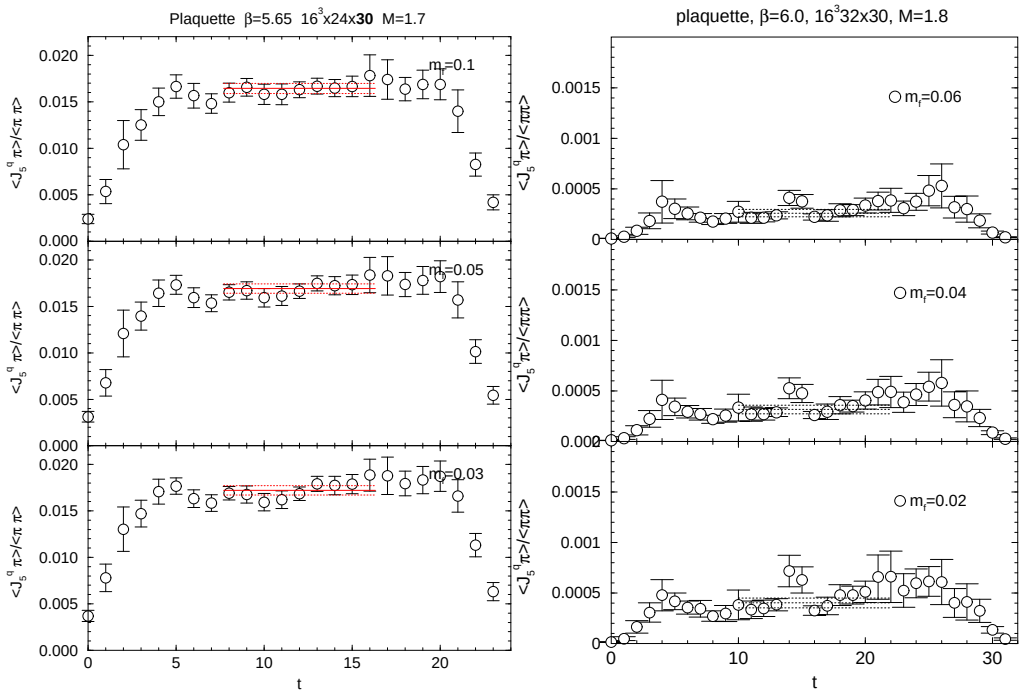

FIG. 1. Ratio of two point functions $< J_{5q}(t)P(0) > / < P(t)P(0) >$ for plaquette action at $\beta = 5.65$, $M = 1.7$ on a $16^3 \times 24 \times 30$ lattice (left) and at $\beta = 6.0$, $M = 1.8$ on a $16^3 \times 32 \times 30$ (right). Lines show constant fit over the fitted range.

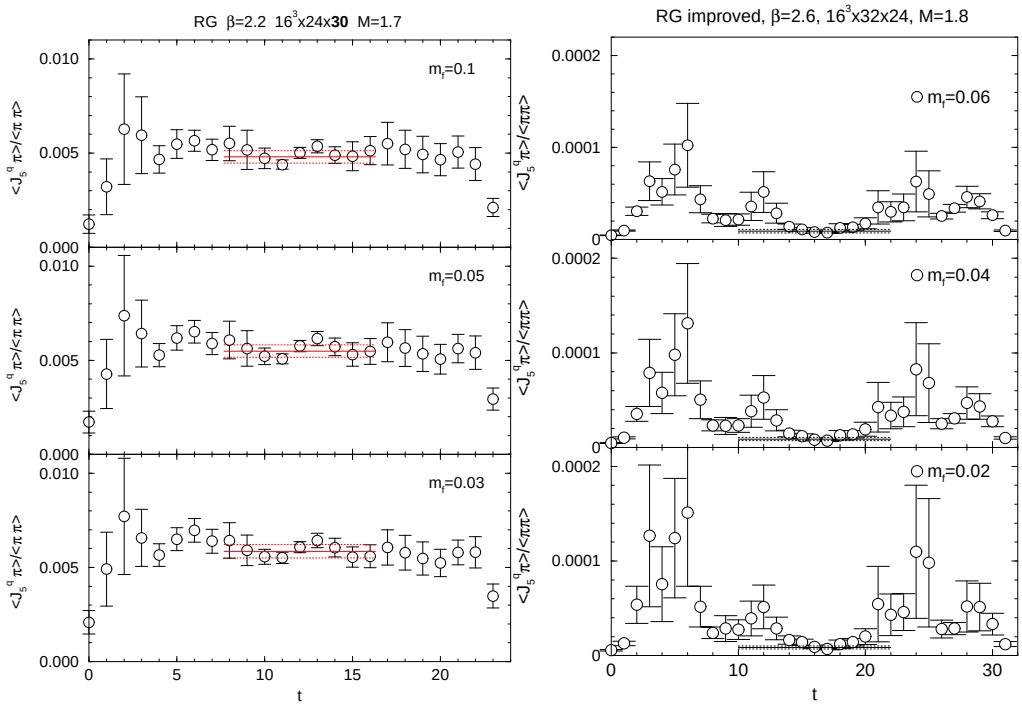

FIG. 2. Ratio of two point functions $< J_{5q}(t)P(0) > / < P(t)P(0) >$ for RG improved action at $\beta = 2.2$, $M = 1.7$ on a $16^3 \times 24 \times 30$ lattice (left) and at $\beta = 2.6$, $M = 1.8$ on a $16^3 \times 32 \times 24$ lattice (right). Lines show constant fit over the fitted range.

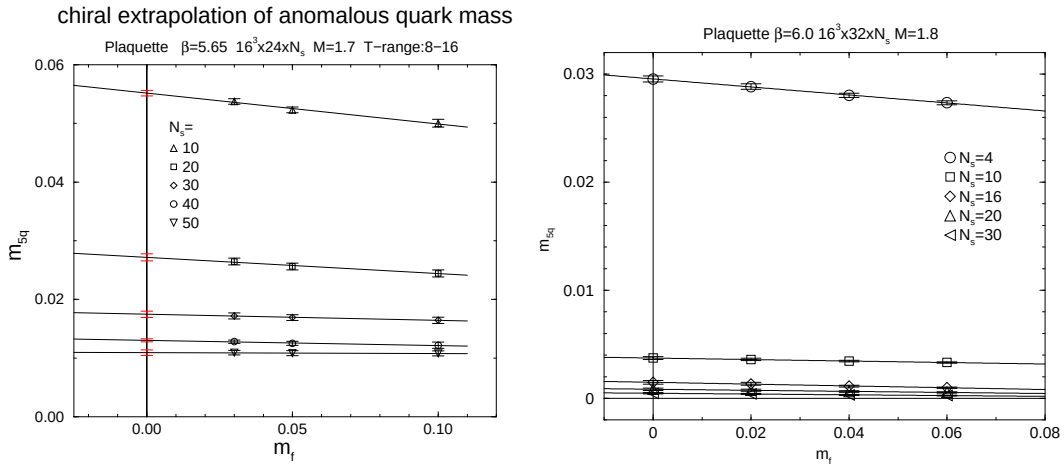

FIG. 3. Anomalous quark mass m_{5q} as a function of m_f for the plaquette action at $M = 1.7$ on a $16^3 \times 24 \times N_s$ lattice in the strong coupling region (left) and at $M = 1.8$ on a $16^3 \times 32 \times N_s$ lattice in the weak coupling region (right).

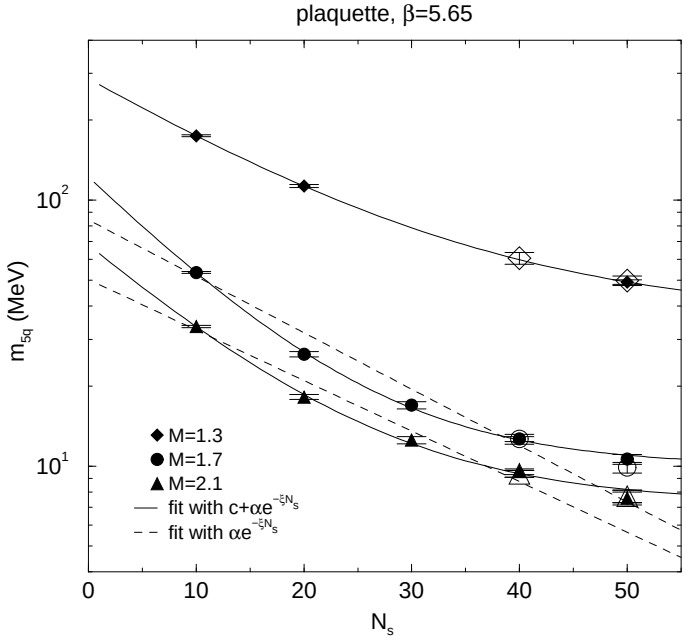

FIG. 4. Anomalous quark mass m_{5q} as a function of N_s in $m_f \to 0$ limit for the plaquette action at $\beta = 5.65$. Filled symbols are data on $16^3 \times 24 \times N_s$ lattice, and open ones on $12^3 \times 24 \times N_s$ lattice. Lines are fits to all the filled points with two functions: $\alpha e^{-\xi N_s}$ (dotted line) and $c + \alpha e^{-\xi N_s}$ (solid line).

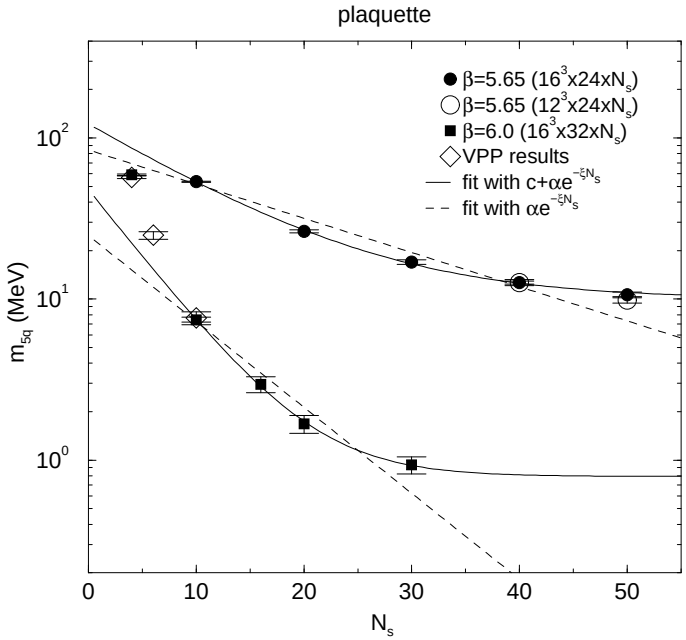

FIG. 5. Anomalous quark mass m_{5q} as a function of N_s in $m_f \to 0$ limit for the plaquette action at weak coupling $\beta = 6.0$ with $M = 1.8$ (filled squares) on a $16^3 \times 32 \times N_s$ lattice. Representative strong coupling results taken at $\beta = 5.65$ and $M = 1.7$ are reproduced from Fig. 4 for comparison (filled and open circles). The results at $\beta = 6.0$ from a previous simulation [20] is also given with open diamonds. Lines are fits to filled symbols with two functions: $\alpha e^{-\xi N_s}$ (dotted line) and $c + \alpha e^{-\xi N_s}$ (solid line).

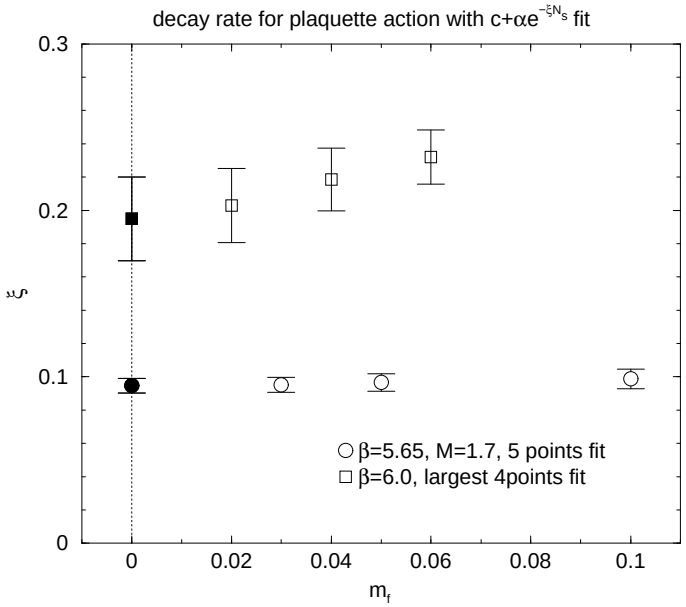

FIG. 6. Decay rate ξ of the anomalous quark mass from the fit with $c + \alpha e^{-\xi N_s}$ for plaquette action. Open circles represent the data in the strong coupling region at $M = 1.7$, $\beta = 5.65$ on $16^3 \times 24 \times N_s$ lattice with five points fit. Open squares are those in the weak coupling region at $M = 1.8$, $\beta = 6.0$ on $16^3 \times 32 \times N_s$ lattice with four points fit.

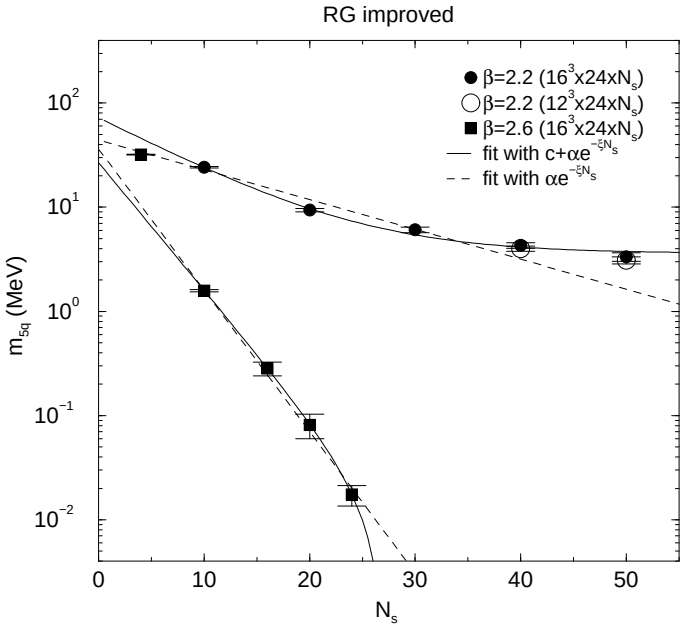

FIG. 7. Anomalous quark mass m_{5q} as a function of N_s in $m_f \to 0$ limit for the RG improved action. Filled circles represent data in the strong coupling region at $M = 1.7$ and $\beta = 2.2$ on $16^3 \times 24 \times N_s$ lattice. Filled squares are those in the weak coupling region at $M = 1.8$ and $\beta = 2.6$ on $16^3 \times 32 \times N_s$ lattice. Lines are fits with two functions: $\alpha e^{-\xi N_s}$ (dotted line) and $c + \alpha e^{-\xi N_s}$ (solid line). Data for $N_s = 10 - 50$ (5 points) and $10 - 24$ (4 points) are used for the fit in the strong and weak coupling.

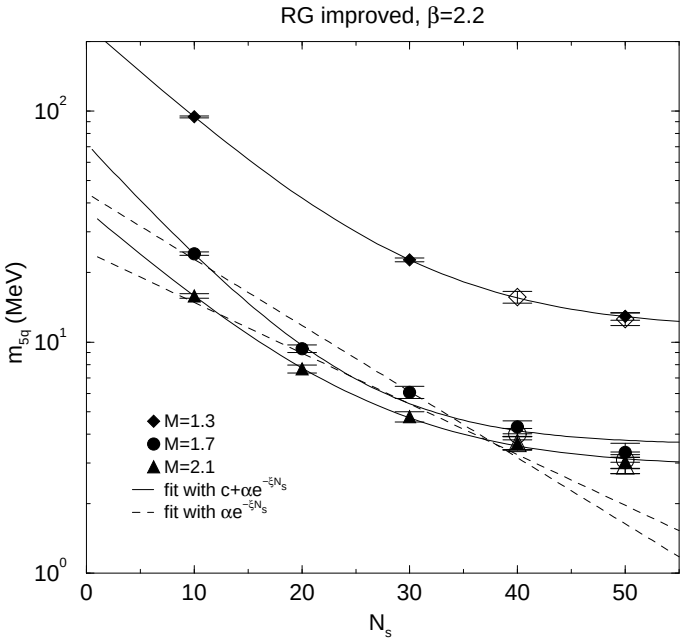

FIG. 8. Anomalous quark mass m_{5q} as a function of N_s in $m_f \to 0$ limit for the RG-improved action at $\beta = 2.2$. Filled symbols are data on $16^3 \times 24 \times N_s$ lattice, and open ones on $12^3 \times 24 \times N_s$ lattice. Lines are fits to all the filled points with two functions: $\alpha e^{-\xi N_s}$ (dotted line) and $c + \alpha e^{-\xi N_s}$ (solid line).

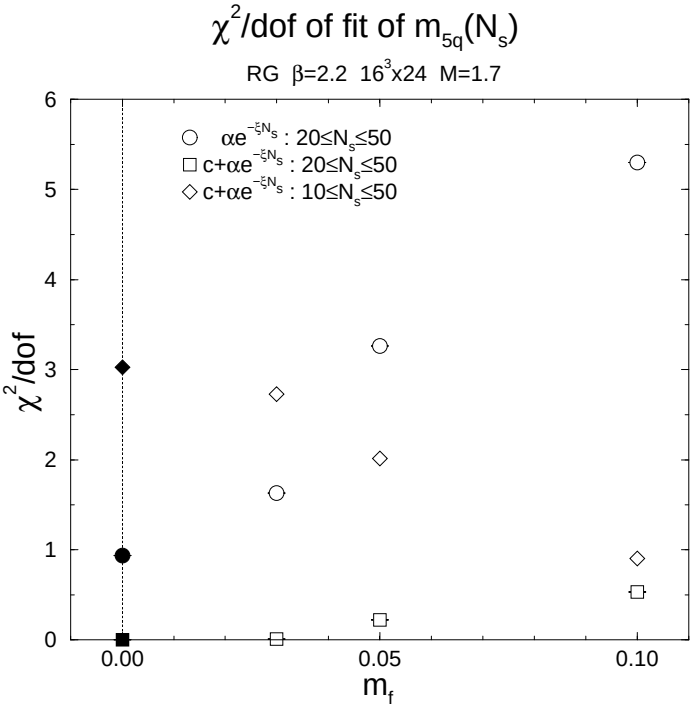

FIG. 9. χ^2/dof in the five and four points fit of m_{5q} data in strong coupling RG action at $\beta = 2.2$, $M = 1.7$. Open circles represent those from the four points fit with simple exponential form $\alpha e^{-\xi N_s}$.

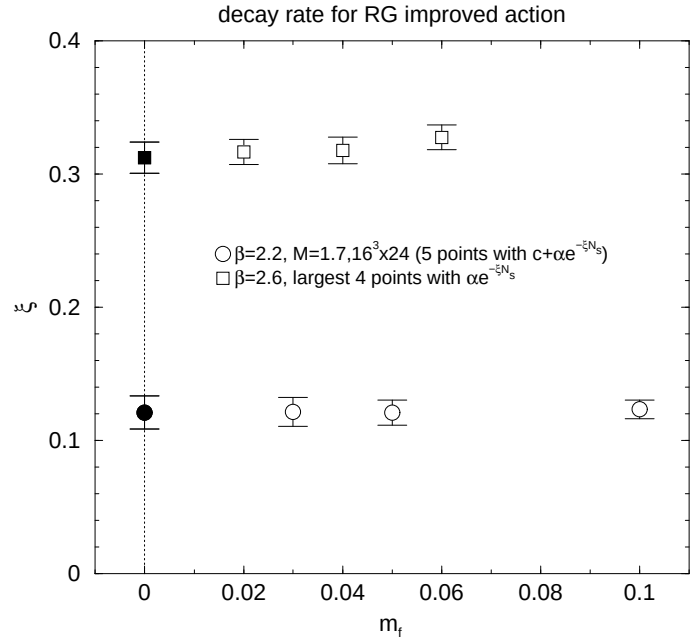

FIG. 10. Decay rate ξ of the anomalous quark mass at each m_f for the RG-improved action. Open circles represent data in the strong coupling region from the five points fit with $c + \alpha e^{-\xi N_s}$ at $M = 1.7$. The open squares are those in the weak coupling region from the four points fit with $\alpha e^{-\xi N_s}$ at $M = 1.8$.

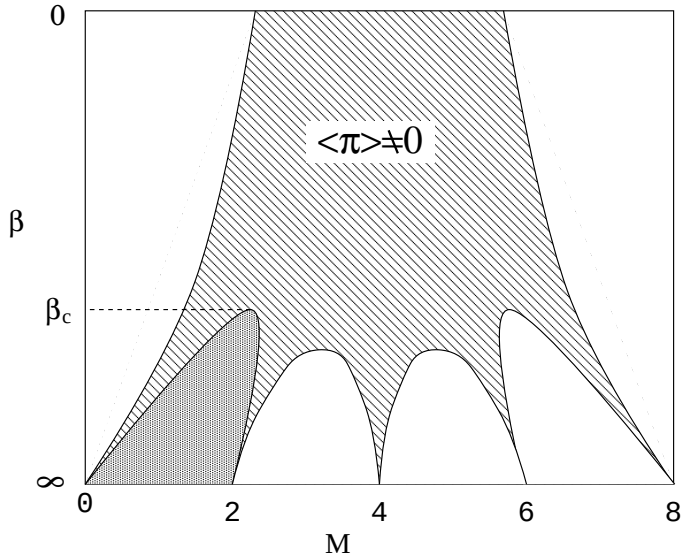

FIG. 11. Phase structure of the four dimensional Wilson fermion system. M represents the fermion mass (domain-wall height). The five cusps at $\beta = \infty$ correspond to the points where subsets of 16 fermions become massless. The shaded area marked by $< \pi > \neq 0$ represents the parity broken phase.

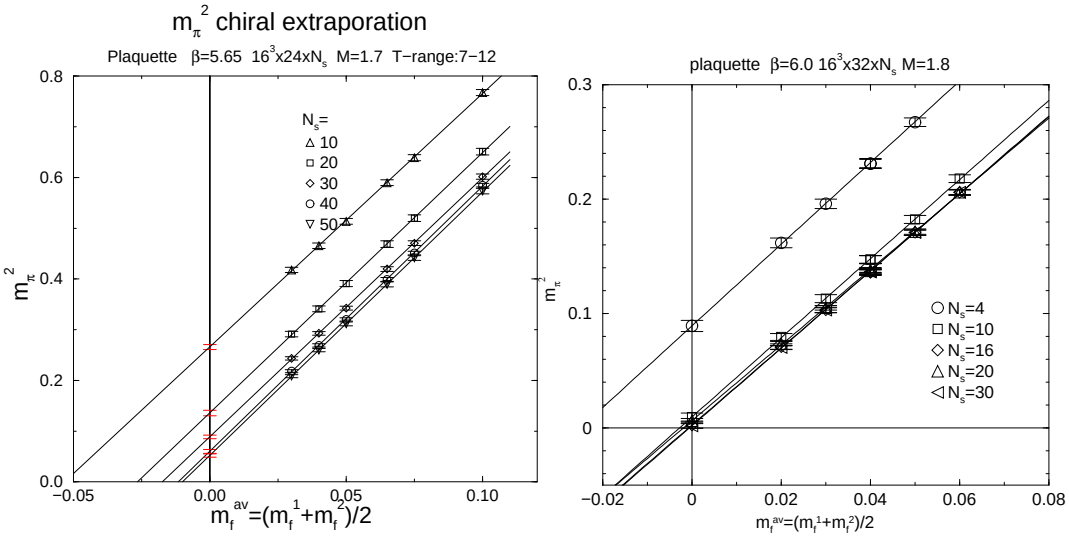

FIG. 12. Pion mass squared as a function of valence quark mass m_f at $M = 1.7, \beta = 5.65$ on $16^3 \times 24 \times N_s$ lattice (left) and $\beta = 6.0$ on $16^3 \times 32 \times N_s$ lattice (right) of plaquette action. Lines are linear fits to those data.

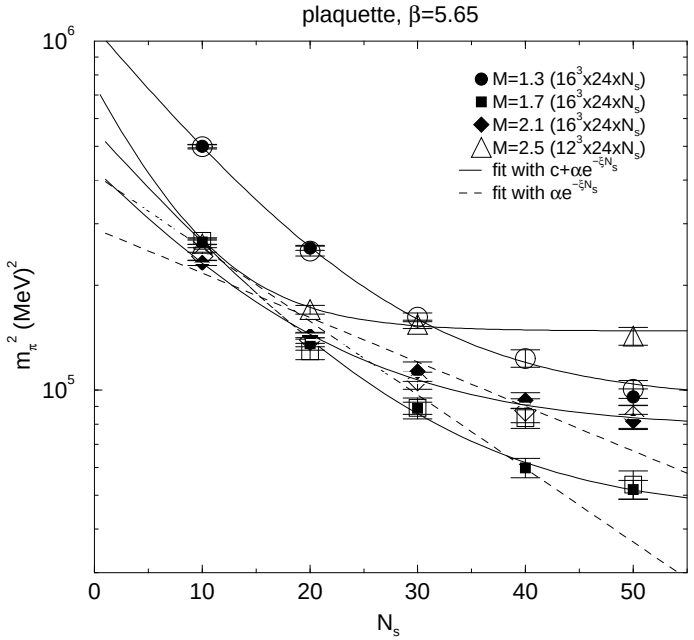

FIG. 13. Pion mass squared at $m_f = 0$ as a function of the extra dimension N_s in the strong coupling region $\beta = 5.65$ for plaquette action. Filled symbols are taken on $16^3 \times 24 \times N_s$ lattice, and open ones on $12^3 \times 24 \times N_s$ lattice. Lines are fits to an exponential with a constant of all five data points on an $N_\sigma = 16$ lattice except for $M = 1.3$ and 2.5 for which data fitted are for $N_\sigma = 12$.

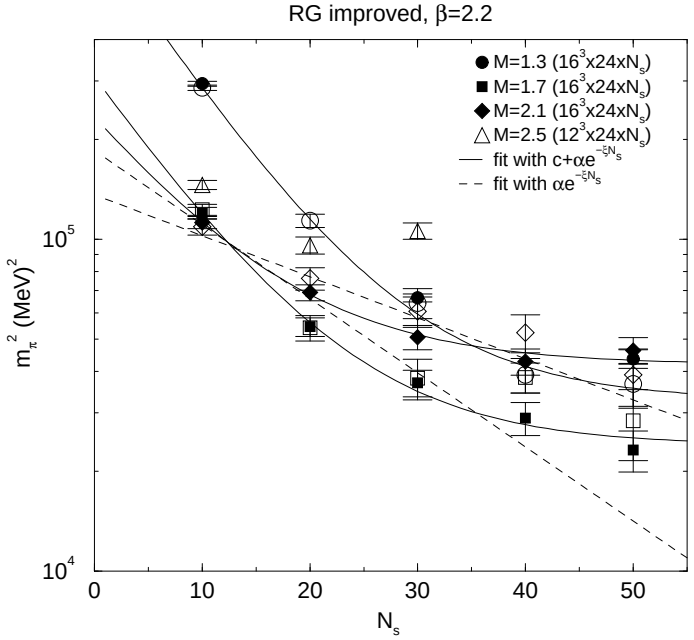

FIG. 14. Pion mass squared at $m_f = 0$ as a function of the extra dimension N_s in the strong coupling region $\beta = 2.2$ for RG-improved action. Filled symbols are taken on $16^3 \times 24 \times N_s$ lattice, and open ones on $12^3 \times 24 \times N_s$ lattice. Lines are fits to a constant and an exponential of all five data points on an $N_\sigma = 16$ lattice except for $M = 1.3$ for which data fitted are for $N_\sigma = 12$.

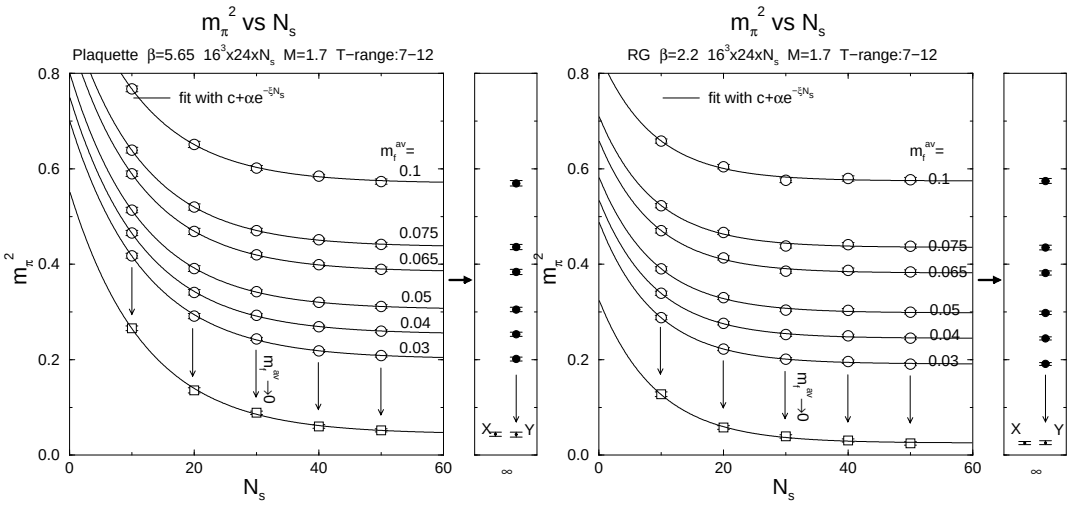

FIG. 15. Pion mass squared as a function of the extra dimension N_s at $M = 1.7$ on $16^3 \times 24 \times N_s$ lattice. The left figure represents the results for the plaquette action at $\beta = 5.65$. The right figure is for the RG action at $\beta = 2.2$. The pion masses derived with two different order of limits $m_f \to 0$, $N_s \to \infty$ are represented with "X" and "Y".

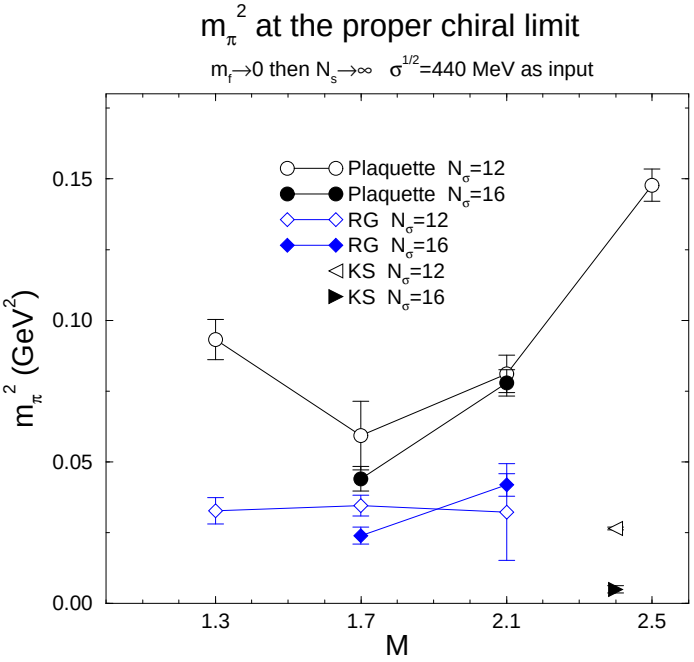

FIG. 16. Pion mass squared as a function of domain-wall height M in the chiral limit $m_f \to 0$, $N_s \to \infty$. The results on $16^3 \times 24$ lattice (open symbols) are compared with those on $12^3 \times 24$ (filled symbols). Open and filled triangles are those from the KS fermion action at $N_\sigma = 12$ and $N_\sigma = 16$ lattice volumes, which represent the pure finite volume effect.

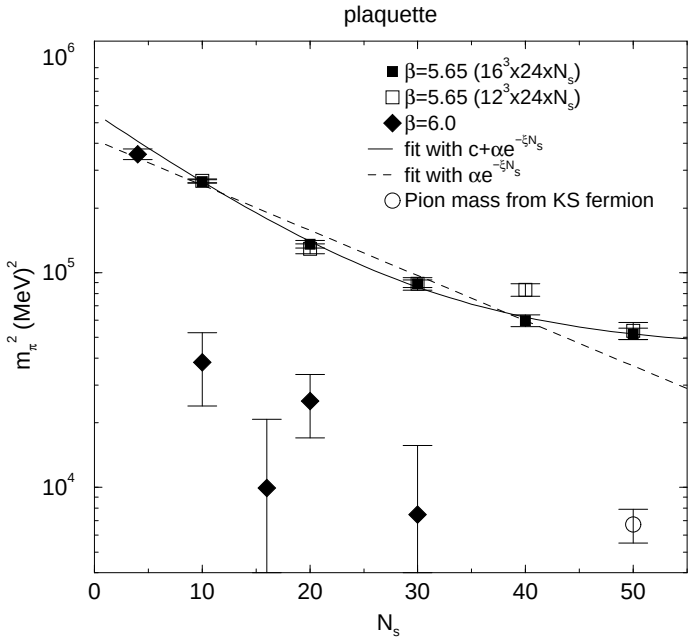

FIG. 17. Pion mass squared at $m_f = 0$ as a function of N_s at $\beta = 6.0$ of plaquette action with $M = 1.8$ (filled diamonds) as compared with those at $\beta = 5.65$ and and $M = 1.7$ (squares). Open circle represents the pion mass from the KS fermion at $N_\sigma = 16$ lattice volume.

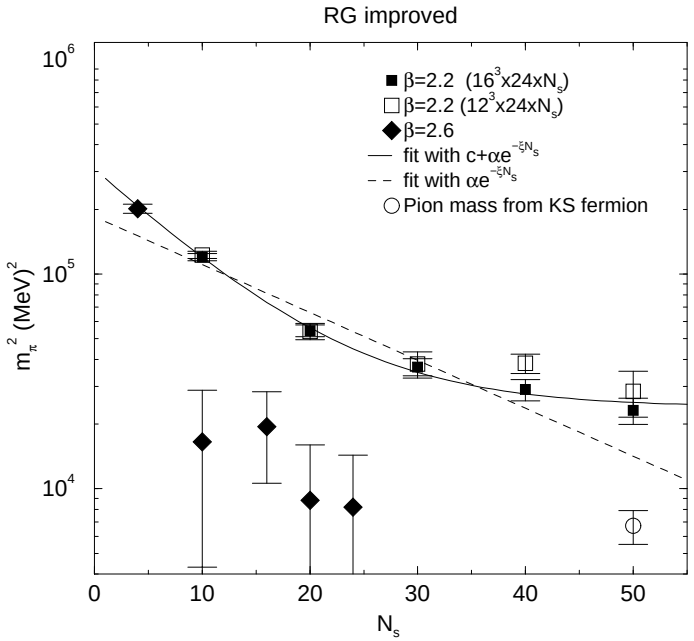

FIG. 18. Pion mass squared at $m_f = 0$ as a function of N_s at $\beta = 2.6$ of RG-improved action with $M = 1.8$ (filled diamonds) as compared with those at $\beta = 2.2$ and and $M = 1.7$ (squares). Open circle represents the pion mass from the KS fermion at $N_\sigma = 16$ lattice volume.